Journal Pre-proof

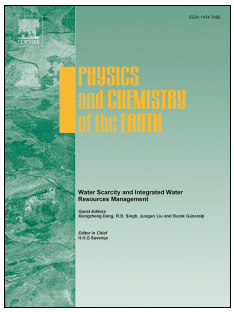

Assessment of multi-source satellite products using hydrological modelling approach

Aiswarya Rani Mahanta, Kishan Singh Rawat, Nirmal Kumar, Szilard Szabo, Prashant K. Srivastava, Sudhir Kumar Singh

PII: S1474-7065(23)00151-1

DOI: https://doi.org/10.1016/j.pce.2023.103507

Reference: JPCE 103507

To appear in: *Physics and Chemistry of the Earth*

Received Date: 19 July 2023

Revised Date: 7 October 2023

Accepted Date: 7 November 2023

Please cite this article as: Mahanta, A.R., Rawat, K.S., Kumar, N., Szabo, S., Srivastava, P.K., Singh, S.K., Assessment of multi-source satellite products using hydrological modelling approach, *Physics and Chemistry of the Earth* (2023), doi: https://doi.org/10.1016/j.pce.2023.103507.

Assessment of multi-source satellite products using hydrological modelling approach

Aiswarya Rani Mahanta[1], Kishan Singh Rawat[1&2], Nirmal Kumar[3], Szilard Szabo[4], Prashant K. Srivastava[5], Sudhir Kumar Singh[3*]

[1]Centre for Remote Sensing and Geoinformatics, Sathyabama Institute of Science and Technology(Deemed To Be University), Jeppiaar Nagar, Chennai, Tamil Nadu, India; Email:aiswaryamahanta777@gmail.com
[2]Civil Engineering Department, Graphic Era (Deemed to Be University), Dehradun, Uttarakhand, India; Email: ksr.kishan@gmail.com
[3]K. Banerjee Centre of Atmospheric & Ocean Studies, IIDS, Nehru Science Centre, University of Allahabad, Prayagraj, Uttar Pradesh, India; Email: nirmalkbcaos15@gmail.com; *Email: sudhirinjnu@gmail.com
[4]Department of Physical Geography and Geoinformation Systems, University of Debrecen, Hungary; Email: szaboszilard.geo@gmail.com; ORCID: 0000-0002-2670-7384
[5]Institute of Environment and Sustainable Development, Banaras Hindu University, Varanasi, India; Email: prashant.just@gmail.com

*Corresponding author's Email: sudhirinjnu@gmail.com

Abstract

Multi-source satellite products performance evaluation for varied geographical locations aids in quantification of hydrological variables and is useful in the strategy making and conservation of the hydrological resources available in a basin. The work was focused on assessing utility of multi-source satellite datasets to obtain the estimation of hydrologic variables and provide solution for areas that are poorly gauged or un-gauged. Assessment of the multi-source-satellite products was performed for the poorly gauged river basin with the help of SWAT concerning the Palar River basin, India. We analysed time series at the monthly, seasonal, and annual scales to quantify surface runoff, water yield, ET, & PET at the calibration site and for the entire basin for the period 2003 to 2021, depending on the common period of availability of all the data sets. SWAT model estimated highest monthly water yield during November–December, with annual water yield being maximum (220 mm in 2010) and average (99 mm), which can be used to understand water resources for irrigation, drinking aspects, and net storage. Average monthly surface runoff patterns were similar for SWAT, TerraClimate, and FLDAS. The FLDAS and SWAT simulated surface runoff show a resemblance in pattern and magnitude for the monthly and annual time series of the average basin scenario. The monthly PET obtained from SWAT and ERA-5 show a similar pattern for the entire basin and at the calibration site. The ET derived from satellite observation has over-predicted the model output at both the calibration site and entire basin.

Keywords: FLDAS; SWAT; ERA-5; MODIS; MERRA-2; Water yield

1. Introduction

Many catchments of interest lack the necessary hydrological data and either poorly gauged or un-gauged (Gehring et al., 2022; Pavelsky et al., 2014; Razavi and Coulibaly, 2013). Understanding the interaction between runoff, evapotranspiration (ET), and prospective evapotranspiration (PET) is essential to comprehending how water moves through ecosystems and how that movement impacts many aspects of our environment. These components are crucial for maintaining the hydrological cycle, in which runoff refers to water that flows off the surface of the ground and into

rivers and streams and ET to the process that combines evaporation and transpiration and returns water to the atmosphere. PET illustrates the maximum water loss that could occur if surplus water is available in the soil. It is useful in the sustainable management of water resources, environmental protection, and climate adaptation. The water budget in a region is based on the balance between these factors, which determines the amount of water that is available for ecosystems, communities, industry, and agriculture. This equilibrium gets affected by changes in land use and the climate. Hydrological models like the Soil and Water Assessment Tool (SWAT) rely on precise ET, PET, and runoff data to anticipate river flow and groundwater recharge. In order to study and manage vital water resources and know how they respond to environmental changes, it is crucial to understand the intricate interaction between runoff, ET, and PET.

Evapotranspiration (ET) is a predominant element of the earth's hydrological system (Irmak, 2008), which illustrates the energy interchange phenomenon that takes place among the biosphere, hydrosphere, and atmosphere (Fan et al., 2018; Li et al., 2016). ET signifies a combined event of evaporation and transpiration, and it is an influential contributor to atmospheric water (Krishna, 2019). It is highly variable depending on soil moisture, vegetation traits, and meteorological parameters, namely solar energy, precipitation, wind velocity, and temperature (Wu et al., 2020; Feng et al., 2016). Therefore, authentic and precise estimation of ET variation is essential for ecosystem modelling, effective irrigation management, environmental assessment, crop yield forecasting, and solar power systems (Singh et al., 2021; Petropoulos et al., 2018; Rawat et al., 2017; Amatya et al., 2014).

ET estimation is a keystone variable for irrigation design and scheduling to achieve high crop yields (Martins et al., 2022; Rawat et al., 2019) and an important input in the hydrological model (Weiland et al., 2011). Actual ET can be estimated from the field by using a lysimeter (Wanniarachchi and Sarukkalige, 2022; Xu et al., 2005), scintillometer (Li et al., 2022; Van Kesteren et al., 2015; Samain and Pauwels, 2013; Solignac et al., 2009), eddy covariance (Paul-Limoges et al., 2020; Moorhead et al., 2019; Anapalli et al., 2018; Widmoser and Wohlfahrt, 2018; Hirschi et al., 2017; Li

et al., 2010), and the Bowen ratio (Martins et al., 2022; Buttar et al., 2018; Zhang et al., 2008). The in-situ methods are time consuming and can cover a small area. However, remote sensing data, namely, Gravity Recovery and Climate Experiment (GRACE), Moderate Resolution Imaging Spectroradiometer (MODIS), and Tropical Rainfall Measuring Mission (TRMM) was used for hydrologic analysis at a synoptic scale for deep insight into water resources (Singh and Gupta, 2016; He et al., 2019; Santra Mitra et al., 2021; Singh et al., 2023a; Singh et al., 2023b). The land surface models (Yassin et al., 2019; Long et al., 2014), and hydrological models (Ghonchepour et al., 2021; Devia et al., 2015; Meng et al., 2014) can be implemented at local, regional, or continental scales for the estimation of hydrologic components for strategy making and conservation of the hydrological resources.

Potential evapotranspiration (PET) is the water mass that can potentially be removed from the earth's surface by evaporation or transpiration if soil water is unlimited (Raza et al., 2022; Xiang et al., 2020; Aouissi et al., 2016). For certain climatic zones, considering the essential inputs and expected assumptions (Paparrizos et al., 2017), four basic approaches for the estimation of PET are as follows: (i) temperature-based, (ii) radiation-based, (iii) a integration of temperature and radiation-based, (iv) mass transfer (Dallaire et al., 2021; Pan et al., 2019; Muniandy et al., 2016; Tabari et al., 2013). Various studies have demonstrated the applicability of hydrologic models for the estimation of different hydrologic components (Kumar et al., 2022; Kumar et al., 2019). The hydrologic models, namely Système Hydrologique Européen (SHE) (Fennell et al., 2022; Sakal et al., 2018; Zhang and Han, 2017; Refsgaard and Clausen, 2010; Abbott et al., 1986), Variable Infiltration Capacity (VIC) (Dayal et al., 2022; Dash et al., 2021; Tesemma et al., 2015; Liang et al., 2003), and Soil and Water Assessment Tool (SWAT) (Adjei et al., 2022; Inayathulla, 2022; Arnold et al., 1998), etc., provide reliable PET estimation. There are several studies where different PET analysis techniques were successfully applied to estimate PET from the basin and plots (Paparrizcos et al., 2017; Lang et al., 2017; Zhao et al., 2013).

The peninsular Indian regions are devoid of any form of precipitation except rainfall, so the hydrology of the basins is generally controlled by climatic events

(Mathew et al., 2022). The Western Ghats' existence has a significant effect on this situation because they cause rain shadow effects in the lower Palar region, which decreases rainfall during the south-west monsoon (Gunnell, 1997). The Palar watershed experiences a hot and humid climate, and due to the lack of substantial snowmelt or glacial input in peninsular India, it heavily depends on seasonal rainfall as the dominant driver of its hydrological patterns (Resmi et al., 2019; 2017; Ramasamy & Varghese, 2018). This indicates that the basin's hydrological dynamics are mostly influenced by seasonal rainfall. The rivers lack water flow during the summer and drought periods, but flood events are more common due to cyclonic events and heavy rainfall during the north-east monsoon (Kamalanandhini and Annadurai, 2022). India is a vast country with a dynamic variation of land surface and climatic conditions, which limits the density of the network of meteorological stations (Mathison et al., 2015; Smakhtin, 2006). on high-resolution reanalysis datasets, for example some of the data sets are- the Climate Forecast System Reanalysis (CFSR) (Kozlov and Ghebrehiwot, 2022; Singh and Saravanan, 2022; Mengistu et al., 2022; Saha et al., 2010), the National Centers for Environmental Prediction (NCEP) and the National Center for Atmospheric Research (NCAR) joint project reanalysis data NCEP/NCAR (Raziei and Parehkar, 2021; Solaiman and Simonovic, 2010; Bromwich and Wang, 2005; Kalnay et al., 1996), NCEP/DOE (Department of Energy) (Singh, Sharma and Juyal, 2018; Kanamitsu et al., 2002), the Japanese 55-year Reanalysis (JRA-55) (Kayaba et al., 2016; Kobayashi et al., 2015; Ebita et al., 2011), the National Aeronautics and Space Administration (NASA) reanalysis product, The Modern-Era Retrospective analysis for Research and Applications (MERRA) (Hamal et al., 2020; Reichle et al., 2017; Rienecker et al., 2011), the European Centre for Medium-Range Weather Forecasts (ECMWF) produced European Environment Agency Interim (ERA-Interim) (Abdollahi et al., 2022; Zolina et al., 2017; Balsamo et al., 2015; Dee et al., 2011), ERA40 (Ghajarnia et al., 2020; Liu et al., 2018; Uppala et al., 2005), and ERA5 (Cantoni et al., 2022; Hersbach et al., 2020). McClean et al. (2021) conducted an evaluation of reanalysis datasets, including ERA-5, MERRA-2, CFSR, and JRA-55, for past floods in Northern England. Their findings indicated that the accuracy of these products varied

geographically, with no single product consistently performing the best across all studied basins.

Wanzala et al. (2022) evaluated the four rainfall reanalysis datasets (ERA-5, ERA-Interim, CFSR, and JRA55) on various temporal scale, i.e., daily, monthly, seasonal, and yearly, over Kenya for the period 1981–2016 and simulated the streams flow. Lindsay et al. (2014) evaluated seven reanalysis products for the data scarce region (the Arctic region) and reported CFSR, MERRA, and ERA-Interim most consistent with the observed. When compared to independent sounding observations over the Tibetan Plateau, Bao and Zhang's (2013) research on the performance of the NCEP-NCAR, NCEP-CFSR, ERA-Interim, and ERA-40 reanalysis datasets revealed that ERA-Interim and CFSR have less root-mean-square (RMS) error and bias. Ma et al. (2008) used reanalysis air temperature data from NCEP-1, 2, and ERA-40 for comparison with observational data over China and discovered that ERA-40 data is superior to NCEP-1 or 2.

Kite et al. (2000) have used various methods for estimating actual ET and transpiration based on satellite data, hydrological models, and field data. They reported that the satellite and FAO-24 methods have the highest variability compared to the models and the field methods, which showed more closeness. There are freely available multi-source satellite products, which are necessary to be evaluated for varied geographical areas in different applications. Hence, we aimed to evaluate the performance of three multi-source satellite products (runoff, ET, and PET) at monthly, seasonal, and annual time scales with the hydrological model (SWAT) for the entire basin and at the calibration site and to identify which products are more reliable and more consistent for the study site.

2. Materials and methods

2.1. Description of the study area

The Palar River Basin (PRB), originating from Nandi Hills, which is a part of the Eastern Dharwar Craton present in Karnataka state, passes through parts of Andhra Pradesh and flows to meet the Bay of Bengal (BoB) at Kancheepuram district of Tamilnadu (Fig. 1). The river's total length is about 348 kilometres; of that, 93

kilometres flow in Karnataka, 33 kilometres within Andhra Pradesh, and 222 kilometres via Tamil Nadu. The major land use/land cover (LULC) in the basin is occupied by agricultural activity (about 90%) and forest (5%) (Mithas et al., 2009). For the year 2020, the major land use class remained agricultural land, followed by forest, savannah, grassland, and settlement (Appendix -I**)**. Alluvial soil is the predominant soil class present in the basin. The region falls under the tropical climatic zone, with an average annual precipitation of 875 mm (Water Plan-Palar River Basin, 1994). The area coverage of the basin is 17,818 km^2. For the basin, 44 meteorological stations are taken into account in a grid format. Nine reservoirs are included in the model input for the basin. The slope of the basin ranges from 0° to about 60°, but the maximum area (94.3%) falls under a 0° to 15° (very gentle) slope. High slopes were observed only in hilly areas of Karnataka. The north-east monsoon season in India, from October to December, is characterised by the highest intensity of rainfall, which is often associated with heavy rainfall caused by cyclonic depressions and storms that often occur in the BoB. The south-west monsoon of India (June to September) contributes to mild precipitation. The Palar River Basin (PRB) is estimated to have an average annual discharge of around 54.6 m^3/s (Palar report, 2015, NWM).

The geomorphology of the basin is denoted by colluvial fill, valley fill, alluvial plains and paleo-channels, flood plains, and residual and structural hills, parts of which have complex faults and folded regions (Ramasamy et al., 2011). The alluvial plains are near the river channel as well as many paleo-channels (Resmi et al., 2016, 2017). In a dendritic and rectangular layout, the drainage network is constructed. (Resmi and Achyuthan, 2019).

Fig. 1 The location map of the study region with meteorological stations, reservoirs, outlet, and calibration point of the PRB.

Appendix -I: LULC statistics of the basin

2.2 Datasets

The work utilized the Shuttle Radar Topography Mission (SRTM) digital elevation model (DEM) of 30 m to generate stream channels, river networks, watersheds, Hydrologic Response Unit (HRU) parameters, and sub-basins. The MODIS Land Cover Product Type MCD12Q1 (1,500 m) was used as LULC map input to create HRUs for defining the curve number (CN) (Sulla-Menashe & Friedl, 2018). For soil properties, the Food and Agricultural Organization (FAO) of the United Nations Harmonized World Soil Database (HWSD) version 1.2, a 30 arc-second raster database (Fisher et al., 2008), was utilised in the research. The SWAT model requires daily or monthly hydro-meteorological data; thus, the ERA5 reanalysis dataset (0.25° resolution) is used to derive daily precipitation (mm) and daily min and max temperature (°C) data (Hersbach et al., 2020). The observed daily stream flow data of Chengalpattu station was acquired from the Central Water Commission (CWC), Government of India, and used for calibration and validation of the model (Table 1).

Table 1 Description of spatial datasets used for the PRB

2.3 Hydrological modelling approach (SWAT)

2.3.1 Water Balance

The SWAT was used to estimate the water balance equation (1):

$$SW_t = SW_0 + \Sigma_i^t{}_{=1} (R_{day} - Q_{surf} - E_a - W_{seep} - Q_{gw}). \quad (1)$$

Where for daily time scale t, SW_t is the final soil water content in the soil (mm), SW_0 is moisture present in the soil at the initial stage (mm), R_{day} is rainfall on the day I in mm, Q_{surf} represents the estimate of surface runoff occurred per day (mm), E_a stands for the total daily ET represent in mm, Wseep represent the estimate of water percolating from the soil to the vadose zone per day (mm), and Qgw represents daily return flow amount in the unit 'mm'.(Neitsch et al., 2005).

2.3.2 Water yield estimation

Water yield is the estimate of water flowing into the mainstream channel from the HRU (Neitsch et al., 2005). An HRU represents a distinct area within a watershed characterised by the identical land use, soil type, and characteristics of slope. It is a

key unit in hydrological modelling. The water yield signifies surface and shallow aquifer conditions with negligible influence from deep groundwater. It quantifies water yield using the following eqn. (2):

$$\text{Water yield} = \text{SURQ} + \text{LATQ} + \text{GWQ} - \text{TLOSS} - \text{Pond abstraction} \quad (2)$$

Where, SURQ is the surface runoff that contributes to stream flow (mm); LATQ (mm) is the lateral flow that contributes to stream flow; GWQ is the water contributed from the shallow aquifer to stream flow (mm); and TLOSS (mm) is the total loss of water from the stream channel by transmission through the stream bed (Neitsch et al., 2005).

2.3.3 Surface Runoff

The surface runoff occurs due to the filling of the pore space available in the soil above its holding capacity by precipitation (Gavrilescu, 2021). The SWAT used the Green and Ampt infiltration method, and the soil conservation system (SCS) to estimate surface runoff. The Green and Ampt infiltration method used precipitation data to estimate the rate of infiltration based on the metric potential of the wetting front and hydraulic conductivity. The SCS curve number method calculates surface runoff by interlinking rainfall-runoff relationships with respect to different soil and land uses and previous soil moisture conditions (Baiamonte, 2019; Neitsch et al., 2009).

SCS curve number-based runoff estimation using equation (3):

$$Q_{surf} = (R_{day} - I_a)^2/(R_{day} - I_a + S) \quad (3)$$

Where Q_{surf} denotes the runoff accumulated (mm), R_{day} is the daily precipitation (mm), and S represents the retention parameter (mm).

2.3.4 Evapotranspiration (ET) estimation

The ET estimation process is carried out in the SWAT model by analysing the amount of water move from earth surface to atmosphere by evaporation and transpiration taking place by the vegetation cover separately. The actual ET calculation procedure of the SWAT model involves evaporating any precipitation

interrupted by the plant canopy, followed by the maximum amount of transpiration and soil evaporation computed using a similar approach suggested by Ritchie (1972). It analyses the ideal conditions for water evaporation from the soil. The evaporative demand that segregates among the distinct soil layers and actual ET for HRU is decreased by the evaporative demand that is not utilised by a soil layer. The actual transpiration is then estimated, which is a function of potential transpiration and soil water availability and is directly associated with the leaf area index that is linked to the plant's developmental stage (Ferreira et al., 2021; Neitsch et al., 2011). The Hargreaves method is implemented for ET and PET estimation because it requires only one input variable, air temperature (Althoff et al., 2019).

2.3.5 Potential Evapotranspiration (PET) estimation

PET estimation can be represented as the rate of ET caused by available energy within a system (Ritchie, 1972). For PET estimation, the Hargreaves method was employed due to its accuracy in energy balance calculation using only precipitation and temperature data, which is less complex than other methods (Ferreira et al., 2021; Chen et al., 2020; Kannan et al., 2008; Wang et al., 2006; Oudin et al., 2005).

Hargreaves method equation (4) expression is as follows:

$$\lambda E_0 = 0.0023 \times H_0 \times (T_{max} - T_{min})^{0.5} \times (T_{mean} + 17.8) \quad (4)$$

where λ denotes latent heat of vaporisation (MJ kg^{-1}), E_0 represents the potential evapotranspiration (mm day^{-1}), H_0 implies extra-terrestrial radiation (MJ m^{-2} day^{-1}), T_{max} and T_{min} denote the maximum and minimum air temperatures for a given day (°C), and T_{mean} represents the mean air temperatures for a given day (°C) (Hargreaves et al., 1985).

2.4 Calibration and uncertainty analysis

The SUFI-2 algorithm was applied for SWAT calibration (Abbaspour et al., 2015), and sensitive parameters were evaluated through t-stat and p-value. The significance of the sensitivity analysis was denoted by p-value (<0.05), where a p-value close to zero denotes the significance of the parameters (Moriasi et al., 2015;

Arnold et al., 2012). The exact match of simulated and observed values is represented by a p-factor of 1 and an r-factor of zero (Tang et al., 2012). The model was calibrated for the period 2003 to 2009 and validated from 2011 to 2013 based on the availability of gauge observation records.

2.5 Satellite-based estimations (runoff, ET and PET)

The FLDAS Global model ET data resolution 9.6 km (0.1° x 0.1°) data sets (NASA Land Information System, LIS) derived runoff data used for comparison. Furthermore, a comparative analysis was performed between the modelled ETs and the MODIS SSEBop monthly global ET data with 1000 m (1/96°) resolution and TerraClimate ET data with 4000 m (1/24°) resolution. For comparative evaluation of satellite observation and SWAT simulated PET, ERA5 reanalysis of Hargreaves PET data with 24-km (0.25° x 0.25°) spatial resolution, TerraClimate PET data with 4000 m (1/24°) resolution, and MERRA2 PET data with 50-km (0.5° x 0.625°) resolution were used (Table 2). The temperature and precipitation anomalies for the entire PRB region were analysed using the ERA5 data.

The study utilised freely available TerraClimate global gridded datasets obtained from Climate Engine, including monthly climate and climatic water balance variables such as runoff, ET, and PET. These data sets were generated by implementing various models and WorldClim climatology data, MODIS-derived topographic features, land surface temperature, cloud cover, Climate Research Unit (CRU) time series data, and the Japanese 55-year Reanalysis (JRA-55) data sets. Using a modified Thornthwaite-Mather climatic water-balance model that incorporates inputs for precipitation, ET, soil moisture, and snowmelt, the publicly available TerraClimate runoff data was created. In order to estimate the precipitation phase, the model adopts an empirical temperature-based approach and permits some of the monthly precipitation and snowmelt to contribute as direct runoff. The Penman-Montieth approach was implemented for evapotranspiration estimation. Hourly and bi-hourly temperature of FLUXNET stations, wind velocity, humidity, and solar radiation observations were utilized for inter-annual ET estimation. Potential evapotranspiration is estimated from

315 ET using the energy balance approach. These data sets are freely available and
316 downloaded for the study from Climate Engine. Abatzoglou et al. (2018) described the
317 data generation process in brief.

318 The FLDAS uses a multi-model approach (Variable Infiltration Capacity, VIC)
319 and Noah Land Surface Model) to estimate surface runoff. It uses the African Rainfall
320 Estimation version 2.0 (RFE2) and The Climate Hazards Group's Infrared
321 Precipitation with Stations (CHIRPS) precipitation data sets, NASA's Modern Era
322 Reanalysis for Research and Applications version 2 (MERRA-2), and NOAA's Global
323 Data Assimilation System (GDAS) data. ET in VIC and Noah was estimated
324 considering the sum of bare soil evaporation, canopy-intercepted evaporation, and
325 vegetation-canopy transpiration with reference to land cover. The Penman-Monteith
326 approach is used in FLDAS for ET and PET estimation. The MOD16 ET datasets are
327 estimated using climate data and remotely acquired vegetation data (Mu et al., 2011).
328 The ET algorithm is based on the Penman-Monteith equation (Monteith, 1965). The
329 MOD16 global ET and PET datasets are accesible at 8-day, monthly, and yearly
330 intervals. The Hargreaves method was used to generate the ERA5 reanalysis PET
331 using ERA5 reanalysis data sets.

332 MERRA2 incorporates hyper-spectral radiation, microwaves, and aerosols as
333 well as a large volume of satellite data. The Catchment Land Surface Model is used in
334 MERRA2, and it includes calculations for land evaporation as part of the surface
335 energy balance (Koster et al., 2000). The Goddard Earth Sciences Data and Information
336 Service Center (DISC) provide hourly data with a 0.625 × 0.5° spatial resolution. All
337 the satellite data used for comparison are open-source datasets downloaded from the climate
338 engine. SWAT model was executed using ERA5 reanalysis rainfall and temperature data,
339 which were also obtained from Climate Engine. Additionally, the SWAT model estimated
340 Evapotranspiration (ET) and Potential Evapotranspiration (PET) using the Hargreaves method.

341 The detailed methodology is described in Fig. 2. For the comparative analysis,
342 satellite-observed water yield data is not available for the study region.

343 **Fig. 2** the detailed methodology used in the quantitative estimation of water balance

components in the PRB using the SWAT model and multi-satellite data.

Table 2 Description of spatial datasets used for comparative analysis at the PRB

2.6. Performance evaluation

The SWAT performance was evaluated using station discharge data. The model was calibrated and validated by using the statistical performance measures coefficient of determination (R^2), Nash-Sutcliffe efficiency (NSE), and Percent Bias (PBIAS). The PBIAS signifies a higher or lower variation of simulation compared to measured data (Moriasi et al., 2007). R^2 indicates the relationship between measured and simulated data, while NSE assesses their agreement on a 1:1 plot. PBIAS aids in evaluating variations between dry and wet years (Gupta et al., 1999). NSE quantifies the relative magnitude of noise (Nash and Sutcliffe, 1970). Whereas PBIAS highlights whether the simulation exhibits greater or lesser variability compared to the measured data (Moriasi et al., 2007).

The model performance equations (5 & 6) are as follows:

$$\text{NSE} = 1 - \left[\frac{\sum_{i=1}^{n}\left(Y_i^{obs} - Y_i^{sim}\right)^2}{\sum_{i=1}^{n}\left(Y_i^{obs} - Y^{mean}\right)^2}\right] \quad (5)$$

$$\text{PBIAS} = \left[\frac{\sum_{i=1}^{n}\left(Y_i^{obs} - Y_i^{sim}\right)*(100)}{\sum_{i=1}^{n}\left(Y_i^{obs}\right)}\right] \quad (6)$$

Where Y_i^{obs} denotes the ith observation, Y_i^{sim} Stands for the value of the ith simulation, Y^{mean} represents the mean value of observed data, and n represents the count of observations for the component being assessed.

The acceptable range is NSE (0.0 to 1.0), R^2 greater than 0.5, and PBIAS near 0 (Moriasi et al., 2007).

The ET and PET estimated with the Hargreaves method (SWAT) were compared with the estimations based on the satellite-based ET and PET. The TerraClimate (for surface runoff, ET, and PET), FLDAS (for surface runoff and ET), MODIS (ET), ERA-5, and MERRA-2 (PET) were used for analysis. Monthly, seasonal, and annual time series analysis was performed at the basin and the calibration site i.e., Chengalpattu.

3. Result and Discussion

3.1. Model performance (SWAT)

For PRB, the sensitive parameters were considered for the model calibration namely: Groundwater delay (days) (GW_DELAY), SCS runoff curve number (CN2), Average slope length (SLSUBBSN), Depth from the soil surface to bottom of layer (SOL_Z), Reservoir surface area when the reservoir is filled to the principal spillway (RES_PSA), Initial reservoir volume (RES_VOL), Volume of water needed to fill the reservoir to the principal spillway (RES_PVOL), Base flow alpha factor (days) (ALPHA_BF), and Average slope steepness (HRU_SLP). The GW delay and CN2 were the most sensitive parameters mentioned in Table 3 for Chengalpattu.

During the calibration period (2003–2009), the model demonstrated satisfactory to good performance, as indicated by several key statistical metrics (Moriasi et al., 2007). These indications show how closely the model's simulated discharge matches actual discharge data (Moriasi et al., 2015). The p-factor, with a value of 0.55, indicates that the model's predicted flow closely aligns with the observed flow. The r-factor measures the relative volume error, and a value of 0.50 signifies that the model's predictions are relatively close to the observed data in terms of volume. R^2 is a widely used statistic to assess the goodness of fit between the model's predictions and observed data. A value of 0.71 indicates a reasonably strong correlation between the two datasets. NSE assesses the relative magnitude of the residual variance compared to the observed data. With an NSE of 0.69, the model's performance is considered satisfactory, as values closer to 1 indicate a better fit. Percent Bias (PBIAS) measures the average tendency of the model's predictions. A value of 19.1 suggests a slight underestimation by the model during the calibration period. In the subsequent validation period, the model's performance was assessed using similar statistical metrics. During validation, the p-factor slightly decreased to 0.47, indicating that the model's predictions still align reasonably well with the observed flow, although to a slightly lesser degree than in the calibration period. The r-factor for validation stands at 0.52, indicating that the relative volume error remains favourable during this period, though it has seen a slight increase. The R^2 value of 0.65 during validation

signifies a good correlation between the model's predictions and observed data, though it's slightly lower than the calibration period. The NSE of 0.63 indicates that the model continues to provide reasonably satisfactory results during the validation period. Here, the PBIAS shows a negative value of -27.5, indicating an overall overestimation by the model during the validation period. The validation period was limited to three years (2011-2013) due to the lack of continuous observed data. This data gap during the validation period could potentially contribute to overestimation issues. Fig. 3 represent the calibration and validation results. Overall, these statistical results during calibration and validation were deemed satisfactory, supporting the model's potential for further applications (Kumar et al., 2022).

The study area is a region of water scarcity. Accordingly, many dams, check dams, and reservoirs were constructed in the area to ensure drinking and irrigation water. These constructions have largely affected the hydrology, and the water is diverted towards Chennai from the Palar Anicut. The Kolar Gold Field and Bharath Earth Movers Limited depend on the water transferred from the PRB (Palar Report, 2015, NWM). Since these factors have affected the flow of the river, the model run was in an ideal condition, and it cannot replicate the exact water distribution of the basin, which is a major limitation in the study area. Hence, the model showed satisfactory to good performance without considering these factors due to the non-availability of the data sets. The limitations of the study are related to the availability of data, as reservoir and lake time series data are not available. Dam data, such as capacity, etc., were collected from reports published by the National Register of Large Dams (NRLD) (Status 1/2018).

Table 3 Description of sensitive parameters for the PRB.

Table 4 SWAT calibration and validation results.

Fig. 3 The model performance evaluation of the SWAT model depicts the model's efficiency as satisfactory to good during the calibration (2003–2009) and validation (2011–2013) periods.

3.2. Variation of Precipitation and Temperature

The spatio-temporal pattern in the average monthly time series of rainfall and temperature (maximum and minimum) distribution was analysed to study the monthly precipitation and temperature variation of the Palar river basin. For the monthly spatio-temporal variation study, the 45 grid points from the ERA5 reanalysis of rainfall and temperature data were analysed.

Appendix- II The monthly variation of temperature and precipitation of PRB.

Based on the data presented in Appendix-II, it can be concluded that over the past four decades, the average monthly temperatures peak in March, April, and May, reaching 33.2°C, 34.93°C, and 35.35°C, respectively, marking the Indian summer season. The temperature declines during the southwest (SW) monsoon period in India and is lowest during the northeast (NE) monsoon, due to heavy rainfall in the study area. During the months of January to April, the average rainfall remains notably low. Subsequently, there is a progressive increase in rainfall during the SW monsoon season, with the highest rainfall occurring during the NE monsoon and cyclone events. From 1984 to 2021, the average maximum daily temperature in the basin was 39.3°C, while the average daily temperature dropped to 12.5°C. Existing literature supports the observation that the period from January to May experiences dry conditions, with the southwest monsoon bringing moderate rainfall while the NE monsoon significantly contributes to precipitation levels in this region (Nigam et al., 2021; Narayanan and Venugopal, 2021; Balathandayutham and Valliammai, 2017).

Appendix- III The spatial distribution of temperature of PRB.

For the entire basin, there is not much fluctuation in temperature. The upper part of the river, which is the hilly region, shows a comparatively lower temperature than the coastal area; the temperature can be seen in a gradually ascending order from the hilly region to the coastal region, which is from the west to east side of the basin. In the summer months (March, April, and May), the coastal meteorological effect and the ocean breeze cause a slight decrease in temperature in the area situated near the Coromandel Coast. In the month of March, the temperature in high-altitude areas rose up to 26 °C, and an increasing pattern in temperature can be seen towards the coast, which reached 28.5 °C in the low-altitude area, but in the coastal region the

460 temperature was about 27.8 °C, as with the increasing distance from the sea, the
461 temperature also increases. Due to coastal meteorological effects, this situation of
462 decreasing temperatures by 1 to 2 °C in the coastal area occurs only during the
463 summer. The spatial temperature variation is shown in Appendix III.

464 **Appendix- IV** The spatial distribution of precipitation over the PRB.

465 Within the basin, precipitation exhibits significant spatiotemporal variation and dual
466 spatial characteristic patterns. From January to May, the precipitation is very low for
467 the whole region. The months of January and February show little rain near the
468 Coromandel Coast. March, April, and May months show precipitation only in the area
469 with the highest elevation (Jawadhu Hills) of the basin. The arrival of the southwest
470 monsoon causes rainfall in the upper part of the basin, while the coastal area does not
471 show any rainfall because of the movement of the monsoon parallel to the
472 Coromandel Coast. Again, August and September show rainfall in the confined high-
473 altitude region. The northeast monsoon (October to December) causes rainfall only in
474 the coastal area. The basin shows dual rainfall in significant seasons as parts of it get
475 rainfall during the SW monsoon while the coastal region is devoid of rainfall. And
476 while the coastal region shows high precipitation during the northeast monsoon, the
477 central and upper basin regions do not experience rainfall (Appendix-IV) (Varikoden
478 and Reji, 2022). During the monsoon, the weighted average maximum and minimum
479 rainfall in the basin are 1,395 and 460 mm, respectively (Water Plan—Palar River
480 Basin, 1994). The effect of the rain shadow region caused by the mountains creates
481 such dual precipitation trends within the basin.

482 Appendix- V The coefficient of variation monthly precipitation and the long-term
483 average monthly precipitation over the PRB.

484 The coefficient of variation (CV) is highest during the month of February, which
485 contributes to the minimum rainfall in the basin, and lowest during the NE monsoon
486 period. The CV with the long-term average monthly precipitation over the PRB region
487 is presented in Appendix V.
488

489 **3.3. Temporal variation of water yield (SWAT)**

The time series water yield was estimated using the SWAT model and it showed a very limited variation in maxima and minima (Fig. 4a). From 2003 to 2021, the highest water yield was observed in December 2014 (116.9 mm), the minimum water yield was observed in the year 2020 and a continuous decreasing trend was observed from January to April. The total average annual water yield for the entire basin was 99.4 mm.

The monthly water yield was in an increasing trend from January to December, and the yearly fluctuation showed an increasing pattern in water yield from 2003 to 2021 (Fig. 4b). The monthly variability showed a similarity with the rainfall pattern for the study area, which is higher for the NE monsoon season. From the analysis of monthly water yield and the monthly rainfall pattern, we found that the water yield and rainfall were the highest during the north-east monsoon period (October to December in Tamil Nadu), causing a maximum rainfall in the study area (Nigam et al., 2021; Narayanan and Venugopal, 2021; Balathandayutham and Valliammai, 2017). The post-monsoon month of January showed a relatively high water yield, while a very low water yield was observed from February to August. It was observed that the maximum value of water yield was obtained in the NE monsoon season (October-December), however, the pre-monsoon season generally becomes drier. The analysis of Fig. 4c showed that the maximum annual water yield was reported for the year 2010, with the average annual of 99.4 mm.

The primary hydrological source for the Palar basin is seasonal rainfall. Peninsular India has no snowmelt or glacial input, therefore the basin's hydrological patterns are mostly influenced by seasonal rainfall and fluctuating cyclonic events. The water yield of the basin is solely derived from these monsoon sources (Ramasamy & Varghese, 2018; Resmi et al., 2017). The fluctuation in water yield within the Palar basin can be attributed to the region's dynamic monsoon conditions, characterized by unpredictable patterns of cyclonic events. Additionally, human activities, such as river water usage, dam operations, water diversion, and storage, are closely dependent to climatic events and further contribute to the variability in water yield.

Fig. 4 Time series of (a) water yield (mm/month), (b) monthly water yield, and (c)

SWAT simulated annual water yield at the calibration station of the basin (2003–2021).

3.4. Analysis of multi-source satellite products versus SWAT

This section deals with the evaluation of multi-source satellite products based hydrological components with the SWAT model-based hydrological component.

3.4.1. Surface runoff based on FLDAS and TerraClimate versus SWAT

For the PRB, the average monthly surface runoff estimated from SWAT, TerraClimate, and FLDAS was 7.6 mm, 8.1 mm, and 9.2 mm, respectively, for the period 2003 to 2021. The results showed that surface runoff ranged from near zero to near 100 mm per month for the PRB (Fig. 5a). The range of time series surface runoff for TerraClimate was 387.9 mm to 0.01 mm, and for FLDAS it was 166.3 mm to 0.3 mm, while the model showed a range of 100.3 mm to 0.01 mm for the entire basin. In comparison to the average basin condition, very high time series runoff was observed at the calibration point; the range for TerraClimate was 755 mm to 0.01 mm, 524.1 mm to 0.01 mm for FLDAS, and 87.4 mm to 0.01 mm for SWAT simulation (Fig. 5b). The surface runoff from satellite observations overestimated the SWAT simulation.

The minimum runoff was close to zero for all the data sets as the river flow fully depends on rainfall in the catchment area. The magnitude and runoff pattern of all the data sets followed a similar pattern with notable differences in magnitude. With its unique capacity to combine many models and data assimilation methods, FLDAS excels at providing accurate runoff estimates in areas with scarce information. Whereas TerraClimate employs a simpler empirical technique, which can result in a loss of accuracy on a regional scale. Watershed hydrology is thoroughly explained using SWAT's process-based approach. In terms of methodology and data sources, these models differ from one another, which produces different runoff magnitudes.

The TerraClimate runoff prediction was the maximum compared to all the datasets during November 2021 and October 2005 and the lowest compared to other data during September 2007, November 2010, and November 2015. The model runoff was highest during April 2005, December 2014, and November 2018. The year 2014

was associated with the very severe cyclonic event of Hudhud, which made landfall over Visakhapatnam, Andhra Pradesh (Das and DSouza, 2020; Chejarla et al., 2017; Murty et al., 2016; Ramuje & Rao, 2015). Cyclone Pyarr in 2005 developed during the SW monsoon season in India and caused heavy rainfall (Naseef & Kumar, 2020; Vasantha et al., 2020; Kotal et al., 2008). In 2008, the eastern coast of India was hit by cyclonic storm Nisha, which affected Andhra Pradesh and Tamil Nadu and caused elevated runoff in late 2008 and early 2009 (Dutta, and Prasad, 2010; Balachandran, and Geetha, 2014; Srivastava, et al., 2011). The year 2018 was associated with cyclone Titli, which had high-speed wind and storm surge that flooded coastal areas due to the heavy rainfall and killed many people (Roul et al., 2022; Nadimpalli et al., 2020; Venkata Rao et al., 2020; Ponnurangam et al., 2019).

The modelled surface runoff for the calibration point was close to 100 mm throughout the study period from 2003 to 2021. The study area is a dry region where the runoff is generated until the soil reaches its saturation limit, and throughout the period of a peak, the runoff is associated with cyclonic events during the northeast monsoon period. The comparative analysis found that both TerraClimate and FLDAS tended to overestimate or occasionally underestimate runoff compared to the model, with FLDAS resulting in closer magnitudes. Some studies have reported similar results (Ahamed et al., 2022; Degefu et al., 2022; Freitas, 2021).

The SWAT simulation runoff is less than the average basin scenario at the calibration point because of water diversion and storage in the upper part. The satellite-observed TerraClimate and FLDAS produce runoff data with the help of a modified Thornthwaite-Mather climatic water-balance model that takes into account precipitation, evapotranspiration, soil moisture, and snowmelt input data. Since the spatial resolution of these global data sets is high and there is a lack of dam, lake, and water extraction data used in the global scale model, variations can be seen when the model is applied to a water-scarce regional area. In this study, open-source data specific to the region was utilized. We have used these specific satellite observations as per the literature reviews which have shown the usefulness of these satellite observations better for the Indian peninsular region (Kushwaha, et al., 2021). Also,

there were no other low-resolution runoff datasets available for this particular geographic area, these data sets were selected for the study.

A moderate increase in runoff was evident due to the South-West monsoon (June to September), as illustrated in Fig. 6(a). The maximum runoff was observed during the NE-monsoon season (October-December), and the river was almost dry during the pre-monsoon season. For the calibration station, the monthly surface runoff was same as the average basin runoff pattern (Fig. 6b). The satellite observations over-predicted the model. The runoff observed during the NE monsoon season (October-December) is governed by the northeast monsoon on the Coromandel Coast.

From the comparative study of the annual surface runoff between the model vs. FLDAS and Terra Climate, from 2003 to 2021, we observed that the surface runoff value of all the data sets followed a similar magnitude and pattern for the basin. The maximum yearly runoff for the whole basin was 41.1 mm, 19.6 mm, and 15.2 mm with TerraClimate, FLDAS, and model, respectively, and the minimum runoff was 1.5 mm, 3.1 mm, and 0.8 mm for the respective data sets (Fig. 7a). The surface runoff derived from FLDAS was closer to the model. At the calibration station, annual TerraClimate runoff varied from 67.6 mm to 2.1 mm, FLDAS varied from 48.9 mm to 3.9 mm, and 11.2 mm to 0.2 mm for the model (Fig. 7b). The available open source high-resolution datasets were primarily designed for large scale study, whereas the calibration point represents a small, localized area near the coast. In the upper region, factors like water utilization, dams, and check dams exert control over runoff, resulting in a notable reduction in flow within the lower basin. This reduction is a critical consideration often overlooked in open-source high-resolution datasets, which typically exclude the influence of human interventions. Given the substantial human impact on the lower basin's flow dynamics, freely accessible high-resolution data, which usually do not account for such factors, may not provide an accurate depiction of the regions reduced flow dynamics. The surface runoff from satellite observations were over-estimated compared to the model. For the calibration point, the magnitude and trend of FLDAS datasets showed a similar pattern to modelled surface runoff. As the monthly time

series observation result stated that for the calibration station, the annual surface runoff also showed over-prediction in both the FLDAS and TerraClimate data.

Fig.5(a) Comparison of monthly runoff from SWAT and freely accessible remote sensing data sets over the entire basin, (b) at the calibration station.

Fig. 6(a) Comparison of the SWAT simulated monthly runoff with freely accessible remote sensing data-sets over the entire basin, and (b) at the calibration station.

Fig. 7(a) Comparison of the SWAT simulated time series plot of runoff with freely accessible remote sensing data sets over the entire basin, and (b) at the calibration station.

The observation leads to the conclusion that, because of their broader spatial scale, TerraClimate and FLDAS data can provide more accuracy for a larger area. FLDAS can be used in an unmodified or unregulated watershed for the Indian scenario for the regional study, but it cannot replace the use of gauge station observed data. Trambauer et al. (2014) reported an underestimation of evaporative fluxes by many global hydrological model data sets, which results in stream flow overestimation in Africa; such overestimation of TerraClimate is seen in the Indian peninsular region in the study.

3.4.2. PET calculated (satellite data) and SWAT

The time series maximum PET of MERRA2 varied from 207.3 mm to 82.4 mm with an average of 146.3 mm. The range of TerraClimate data (PET) varied from 131.8 mm to 64.9 mm, with an average of 97.6 mm per month. For the ERA5 and model result, the maximum values were 178.7 mm and 189.1 mm, and the minimum values were 76.0 mm and 90.9 mm, with an average of 133.2 mm and 131.8 mm, respectively, for the basin. The PET from ERA5 was closer to the model. The TerraClimate is under-predicted, and MERRA2 is over-predicted with a similar magnitude and pattern (Fig. 8a). Different approaches and input data for MERRA-2, TerraClimate, ERA5, and SWAT are used to estimate PET (Ansari, et al., 2022). Other data sets, however, used the Penman-Monteith technique and a variety of inputs, as detailed in Section 2.5. For

PET estimates in ERA5 and SWAT, the Hargreaves approach is utilized with ERA5 reanalysis input data. As a consequence, the results are closely matched.

The monthly PET for the basin and calibration station did not have much variation. The MERRA2 PET varied between 207.9 mm to 78.0 mm with an average of 145.3 mm; the PET of TerraClimate varied between 136.6 mm to 66.5 mm with an average of 101.6 mm, and the ERA5 and model PET ranged between 190.1 mm to 78.2 mm (an average 140.9 mm) and 189.1 mm to 90.2 mm (an average 131.9 mm) respectively. Under prediction of TerraClimate and over-prediction of MERRA2 were observed throughout the study period (2003–2021) (Fig. 8b).

The summer months of the basin showed a higher PET value, and before the arrival of the southwest monsoon, the PET started to decline, as a drastic fall in PET was observed from May to June, which was 24.7 mm, 14.9 mm, 24.5 mm, and 34.6 mm for MERRA2, TerraClimate, ERA5, and model, respectively. The decreasing pattern continued from July to November (154.0 mm, 101.1 mm, 139.2 mm, and 124.4 mm in July to 103.0 mm, 73.1 mm, 97.1 mm, and 101.7 mm, in November, respectively, for MERRA2, TerraClimate, ERA5, and model). From November to December, the lowest PET was estimated, and it started increasing in January (127.2 mm, 75.53 mm, 114.9 mm, 120.9 mm, respectively for MERRA2, TerraClimate, ERA5, and model) to February (145.1 mm, 92.6 mm, 127.4 mm, 129.7 mm respectively for MERRA2, TerraClimate, ERA5, and model) and a drastic increase was observed when summer approached from February to March (190.1 mm, 113.7 mm, 162.0 mm, 167.2 mm, respectively for MERRA2, TerraClimate, ERA5, and model) (Fig. 9a). The monthly PET from ERA5 was closer to the model. The monthly pattern of PET at the calibration station was a closer match to the basin PET scenario. There was no relevant change observed between the whole basin and calibration station observations (Fig. 9b).

The annual variation of PET from 2003 to 2021 showed an almost constant pattern for all the data sets except MERRA2, which showed a slightly decreasing pattern for the study period. The ERA5 Hargreaves PET results matched well with the model PET with ERA5 temperature and rainfall input. The ERA5 and model PET

showed similarities, and TerraClimate under predicted and MERRA2 slightly over-predicted for the entire study period (Fig. 10a). The calibration station showed an over prediction of ERA5, MERRA2, and under-prediction of TerraClimate data (Fig. 10b).

Similarities between the ERA5 and model PET were found, and over the entire study period, TerraClimate underpredicted and MERRA2 slightly overpredicted. Based on the literature, many researchers implemented ERA5 and MERRA2-derived PET (Nouri and Homaee, 2022; Scherrer et al., 2022; Dahri et al., 2021; Ochege et al., 2021).

Weiland et al. (2012) did a comparative study to select the best method to estimate daily global PET by applying CFSR reanalysis data in the hydrological model. Srivastava et al. (2013) used ECMWF ERA-Interim data and NCEP data to estimate the PET. ERA5 and MERRA2 data sets were used for PET estimation (Nouri and Homaee, 2022; Scherrer et al., 2022; Dahri et al., 2021; Ochege et al., 2021). Trambauer et al. (2014) did a comparative study between the PET estimated by the ECMWF reanalysis datasets, ERA-Land and ERA-Interim, and satellite-based products GLEAM and MOD16 with a continental version of the global hydrological model PCR-GLOBWB. This study also reported that the majority of continental or global scale hydrological models underestimate evaporative fluxes, while the land-surface models reported overestimation. The ERA5 reanalysis PET data best represented the PRB area of peninsular India.

Fig. 8(a) Comparison of the SWAT simulated time series plot of PET with freely accessible remote sensing data sets over the entire basin, and (b) at the calibration station.

Fig.9 (a) Comparison of the monthly PET from SWAT simulation and freely accessible remote sensing data sets over the entire basin, and (b) at the calibration station.

Fig. 10(a) Describe the comparison of the annual time series plot of Potential Evapotranspiration of SWAT simulated with freely accessible remote sensing data sets over the entire basin(1984-2021), and (b) at the calibration station(1984-2021).

3.4.3 ET calculated (satellite data) and SWAT

Remote sensing also has certain limitations, such as poor temporal resolution,

global algorithms for data retrieval, and signal interference during the time of acquisition that affects the data quality (Zhang and Kimball, 2016). In this study, Terra climate, FLDAS, and MODIS ET on a time series basis were compared with model ET for the period 2003–2021. The TerraClimate ET was at its maximum during September 2009 (137.872 mm) and minimum in February 2017 (1.004 mm), with an average for the total study period of 70.8 mm. The maximum FLDAS ET was 148.77 mm (September 2010); the minimum was 10.68 mm (April 2014), with an average of 83.15 mm. The maximum MODIS ET was 134.95 mm (May 2012), the minimum was 15.41 mm (February 2015), and the average was 73.25 mm. The model ET ranged from a maximum of 130.80 mm (May 2005) to a minimum of 9.7 mm (February 2011), with an average of 59.93 mm. All the data sets showed similar magnitudes and an increasing or decreasing pattern throughout the study period. All the data sets showed ET overestimation; the MODIS data sets had the closest match with model ET for the study period (Fig. 11a).

The ET value at the calibration station was higher than the average basin ET (Fig.11b). The MODIS ET at the calibration station varied between 164mm and 15.33mm, the FLDAS ET ranged from 152.64mm to 9.79mm, the TerraClimate ET varied between a maximum of 172.96mm and a minimum of 1.36mm, and the model showed 144.31mm maximum and 8.84mm minimum for the entire study period (2003–2021).

A comparison of a long-term average monthly ET was done from 2003 to 2021 among the modelled ET and remote sensing acquired Terra Climate, FLDAS, and MODIS data sets. The average monthly ET was highest from July to October for all the data sets. FLDAS showed a constant high ET value during November and December, however, the ET pattern decreased for other data sets during this period. The months of January, February, March, and April showed less evapotranspiration for all the simulated and remote sensing data sets (Fig.12a). Both the calibration station and average basin ET value matched closely and followed a similar increasing and decreasing pattern for the months. The MODIS data set was a closer match with the model monthly ET (Fig.12b).

The yearly ET takes place from 2003 to 2021, and the calculated result for the study showed a similar magnitude and pattern for all the data sets and SWAT observed results for the whole basin as well as for the calibration station, as shown in Fig.13a and Fig.13b. All the data sets over predict the ET than the SWAT simulated result. Remotely detected ET data has been utilised in many studies around the globe to enhance flood forecasting, discharge simulation, and agricultural yield simulation (Zhang et al., 2016). Few uncertainties appear because of a fragmentary vegetative cowl, model falsifications, coverage, and inputs (Dile et al., 2020).

The acquisition method, spatial scale, and input data used in the SWAT simulation and ET from satellite observation were different. Due to the research area's predominance in agriculture, SWAT's simulated ET exhibited a greater portrayal of the agricultural season. The SWAT-generated ET was best matched by the MODIS, followed by the FLDAS. The difference between MODIS and SWAT simulated ET could be caused by acquisition technique, as MODIS ET was estimated considering climatic conditions and remote sensing-derived vegetation cover data but did not take into account land use, slope, and soil characteristics.

The regional model simulated ET compared with freely available global data sets and reported the fluctuation of the global data set with respect to the regional model (Filgueiras et al., 2022). ET was reported as the most uncertain flux of water balance and variation of the global and regional observed data sets seen in these studies. So, to minimise model simulation error, the remote sensing ET should pass through fastidious evaluation and comparison with other available sources before being implemented in water resource estimation (Ahamed et al., 2022). The TerraClimate reported satisfactory performance for the hydrological components analysis (Wiwoho and Astuti, 2022; Abatzoglou et al., 2018). McNally et al, (2016) reported high accuracy of FLDAS surface runoff and ET with the field observation in severe drought hit Ethiopia and Southern Africa. Pervez et al, (2016) reported good correlations between FLDAS with Operational Simplified Surface Energy Balance (SSEBop) ET over East and Southern Africa. Many studies reported the usability of FLDAS for hydrological components (Li et al., 2020; McNally et al. (2016) reported

high accuracy of FLDAS surface runoff and ET with field observation in severe drought-hit Ethiopia and southern Africa. Pervez et al. (2016) reported good correlations between FLDAS and Operational Simplified Surface Energy Balance (SSEBop) ET over East and Southern Africa. Many studies have reported the usability of FLDAS for hydrological components (Li et al., 2020; McNally et al., 2019). MODIS ET has been implemented in many research works for local-scale hydrological studies (Parajuli et al., 2022; Jiang et al., 2022; Lu et al., 2022; He et al., 2019; Zhang et al., 2019; Abiodun et al., 2018).

Fig.11(a) comparison of the time series plot of the evapotranspiration of the SWAT simulation with freely accessible remote sensing data sets over the entire basin, and (b) at the calibration station.

Fig.12(a) The comparison of the monthly plot of Evapotraspirtion of SWAT simulated and freely accessible remote sensing data-sets over the entire basin, and (b) at the calibration station.

Fig.13(a) The comparison of the annual time series plot of Evapotraspirtion of SWAT simulation with freely accessible remote sensing data-sets over the entire basin, and (b) at the calibration station(2003–2021).

4. Total water balance components

The SWAT model for the entire basin estimated a long-term average annual rainfall value of 830.3 mm for the simulation period of 1984 to 2021. The region is situated in a tropical climatic zone, so the region is devoid of snowfall, which is seen in model simulation, as snowfall, snow melt, and sublimation are zero in SWAT output. The basin is occupied by four major aquifer systems, such as the basement gneissic complex, gneiss, charnockite, and alluvium. The water percolation in lateral soil is 3.20 mm, for the shallow aquifer 6.07mm, and 1.31mm for the deep aquifer regions. The evaporation from the shallow aquifer was 21.19 mm. The total aquifer recharge was 26.61mm. Water percolation out of the soil was 26.69 mm.

For this study, ERA-5 reanalysis datasets were taken into consideration because of their better performance in comparison to other available reanalysis products in the Indian region (Mahto and Mishra, 2019). According to recent research, the ERA5 rainfall data was the most accurate when choosing rainfall input for the SWAT model

in humid regions (Ougahi and Mahmood, 2022; Mohammadi and Sharafi, 2022). Tarek et al. (2020) reported that the performance of hydrological models based on ERA5 is equivalent to the use of observational data for the majority of North America. Many studies have evaluated the performance of ERA-5 global reanalysis, ET, and PET. Wang et al. (2022) found that ERA5 performed better than other gridded PET datasets at the watershed scale, with a higher NSE and a lower PBIAS. According to Pelosi et al. (2020), ERA5 reanalysis can successfully substitute the absence of observed weather parameters for the regional estimation of ET. The ERA5 PET was estimated using the Hargreaves method, and the SWAT model simulated for ET and PET using the same algorithm for the study. Our scope of the study was to analyse various open-source satellite products on a regional scale (non-perennial basin scale) for the peninsular Indian region. Among the evaluated products for the peninsular Indian region, FLDAS surface runoff, ERA5 PET, and MODIS ET are found to be the most accurate satellite datasets for capturing the area's environmental characteristics. The seasonal representation of the basin shows similarities in water yield and surface runoff in all the data sets. The runoff and water yield are at their maximum during the NE monsoon season (Fig. 14.a). The seasonal ET of the basin is greatest in the summer (April-June), and the PET is highest in both the SW and NE seasons (Fig. 14.b).

Pandi et al. (2022) estimated the ET in the Chittar catchment in Tamil Nadu, India, and discovered that it was highest in the months of January to March and lowest in the months of June to September, with the help of the SWAT model. They further suggested that rainwater harvesting structures may help in mitigating floods and droughts in the catchment. The monthly runoff for the Koyna river basin in Maharashtra, India, was estimated, and the result concluded that water balance and water yield information aid in sustainable water resources management at the basin-level scale (Landage and Keshari, 2022). Sao et al. (2020) used the SWAT model to determine the annual mean water yield and different components of the water balance (including annual average evapotranspiration, groundwater flow, surface runoff, and lateral flow) in the Pursat River Basin of Cambodia, which is distinguished by a tropical monsoon climate and forested terrain. They found that the annual average

water yield and other elements of the water balance could be most accurately estimated using the NSE and RSR objective functions. Kumar et al. (2018) applied the SWAT model and future LULC and reported that the hydrological change in a basin was not correlated with LULC change for the Tons River, Madhya Pradesh, India. Gupta et al. (2020) applied the SWAT model and trend analysis method for the upper Sabarmati River basin in India and observed a significant decreasing trend in runoff, PET, and ET due to the decreasing trend of precipitation. Kumar et al. (2022) implemented the SWAT model, along with CMIP6 climate projection and satellite altimetry data, to analyze the Himalayan River Basin and warned about high-frequency elevated flow events of short duration. Visakh et al. (2019) implemented the SWAT model to estimate the components of the long-term water balance for the Mahanadi, Brahmani-Baitarani, Hooghly River, and other minor river basins in eastern India. Significant inter-annual fluctuations in evapotranspiration and surface runoff fractions were observed due to the variability in rainfall. A literature study of the SWAT model states that the base flow simulation can be modified with a coupled model with SWAT (Yuan and Forshay, 2021) or by considering recession characteristics (Lee et al., 2018).

5. Conclusions

The proposed approach can be beneficial for poorly gauged and un-gauged basins for prediction and evaluation of model output with reanalysis data. The SWAT model calibration and validation statistical measures showed satisfactory model performance. The novelty of the study lies in the utility of multi-source satellite observations for the estimation of the hydrologic components and their comparison with the hydrologic model output for a peninsular river basin where the majority of the rain is received during the northeast monsoon. The SWAT model was selected to capture the surface hydrology and quantified the water yield, surface runoff, ET, and PET for the entire basin. Water yield and surface runoff hydrologic variables were well matched to the monthly rainfall trend (northeast monsoon) in the basin. The maximum PET was observed during the summer period, and higher ET was observed during both the monsoon periods (northeast and southwest monsoons). For the study

period, the total average annual water yield for the entire basin was reported as 99.44 mm. The TerraClimate showed over-prediction for certain times during the study, while FLDAS and model results were close to the total basin scenario. Both the FLDAS and TerraClimate had over-predicted at the calibration station. The area receives majority of rainfall during the north-east monsoon hence, the runoff was maximum during the season. The PET did not show much variation with regard to the basin and the calibration point. The Hargreaves PET for the model and ERA5 showed a good resemblance for the study period (1984 to 2021). In comparison to the model, TerraClimate under-predicted and MERRA2 over-predicted with comparable magnitude and pattern. Hence, this study outlined the importance of the freely accessible multi-source satellite products for the data scarce region and aid in planning and management of the water resources of similar types of basins.

The study recommends further water management studies in the upper palar region, future hydro climatic condition prediction, and a better base flow management study (as from the SWAT simulation result, it is observed that it lacks base flow prediction). Future research should be done while taking the base flow of each sub-basin into account.

Acknowledgments: This work has been carried out at the K. Banerjee Centre of Atmospheric and Ocean Studies (KBCAOS), IIDS, Nehru Science Centre, University of Allahabad, India and we are thankful to the Coordinator of KBCAOS for providing the lab and infrastructural support. We gratefully acknowledge the director of research and all staff at the Centre for Remote Sensing and Geoinformatics, Sathyabama Institute of Science and Technology. Szabo S. was supported by the TKP2021-NKTA-32 (NKFI) project.

References

Yuan, L., & Forshay, K. J. (2021). Enhanced stream flow prediction with SWAT using support vector regression for spatial calibration: A case study in the Illinois River watershed, US. *PloS one*, *16*(4), e0248489.

Lee, J., Kim, J., Jang, W. S., Lim, K. J., & Engel, B. A. (2018). Assessment of baseflow estimates considering recession characteristics in SWAT. *Water*, *10*(4), 371.

Liang, Z., Tang, T., Li, B., Liu, T., Wang, J., & Hu, Y. (2018). Long-term streamflow forecasting using SWAT through the integration of the random forests precipitation generator: case study of Danjiangkou Reservoir. *Hydrology Research*, *49*(5), 1513-1527.

Mahto, S. S., & Mishra, V. (2019). Does ERA-5 outperform other reanalysis products for hydrologic applications in India?. *Journal of Geophysical Research: Atmospheres*, *124*(16), 9423-9441.

Ougahi, J. H., & Mahmood, S. A. (2022). Evaluation of satellite-based and reanalysis precipitation datasets by hydrologic simulation in the Chenab river basin. Journal of Water and Climate Change, 13(3), 1563-1582.

Tarek, M., Brissette, F. P., & Arsenault, R. (2020). Evaluation of the ERA5 reanalysis as a potential reference dataset for hydrological modelling over North America. *Hydrology and Earth System Sciences*, *24*(5), 2527-2544.

Pelosi, A., Terribile, F., D'Urso, G., & Chirico, G. B. (2020). Comparison of ERA5-Land and UERRA MESCAN-SURFEX reanalysis data with spatially interpolated weather observations for the regional assessment of reference evapotranspiration. *Water*, *12*(6), 1669.

Wang, C., Si, J., Li, Z., Zhao, C., Jia, B., Celestin, S., ... & Zhu, X. (2022). Evaluation of three gridded potential evapotranspiration datasets for streamflow simulation in three inland river basins in the arid Hexi Corridor, Northwest China. *Journal of Hydrology: Regional Studies*, *44*, 101234.

Pelosi, A., Terribile, F., D'Urso, G., & Chirico, G. B. (2020). Comparison of ERA5-Land and UERRA MESCAN-SURFEX reanalysis data with spatially interpolated weather observations for the regional assessment of reference evapotranspiration. *Water*, *12*(6), 1669.

Mohammadi Ghaleni, M., & Sharafi, S. (2022). Evaluation of CRU TS4. 05 and ERA5 Datasets Accuracy to Precipitation, Temperature and Potential Evapotranspiration in Different Climates across Iran. *Iranian Journal of Irrigation & Drainage*.

Abatzoglou, J. T., Dobrowski, S. Z., Parks, S. A., & Hegewisch, K. C. (2018). TerraClimate, a high-resolution global dataset of monthly climate and climatic water balance from 1958–2015. *Scientific data*, *5*(1), 1-12.

McNally, A., Arsenault, K., Kumar, S., Shukla, S., Peterson, P., Wang, S., ... & Verdin, J. P. (2017). A land data assimilation system for sub-Saharan Africa food and water security applications. *Scientific data*, *4*(1), 1-19.

MODIS Global Evapotranspiration Project (MOD16), http://www.ntsg.umt.edu/project/modis/mod16.php

Abbaspour, K. C. (2015). SWAT calibration and uncertainty programs. *A User Manual*, 17-66.

Abbaspour, K. C., Johnson, C. A., & Van Genuchten, M. T. (2004). Estimating uncertain flow and transport parameters using a sequential uncertainty fitting procedure. Vadose zone journal, 3(4), 1340-1352.

Abbaspour, K. C., Rouholahnejad, E., Vaghefi, Srinivasan, R., Yang, H., & Kløve, B. (2015). A continental-scale hydrology and water quality model for Europe: Calibration and uncertainty of a high-resolution large-scale SWAT model. Journal of hydrology, 524, 733-752.

Abbott, M. B., Bathurst, J. C., Cunge, J. A., O'Connell, P. E., & Rasmussen, J. (1986). An introduction to the European Hydrological System—SystemeHydrologiqueEuropeen,"SHE", 1: History and philosophy of a physically-based, distributed modelling system. Journal of hydrology, 87(1-2), 45-59.

Abdollahi, B., Alidoost, F., MoshirPanahi, D., Hut, R., & van de Giesen, N. (2022). ERA5 and ERA-Interim Data Processing for the GlobWat Global Hydrological Model. *Water*, *14*(12), 1950.

Abiodun, O. O., Guan, H., Post, V. E., &Batelaan, O. (2018). Comparison of MODIS and SWAT evapotranspiration over a complex terrain at different spatial scales. *Hydrology and Earth System Sciences*, *22*(5), 2775-2794.

Adjei, F. O., Obuobie, E., Adjei, K. A., &Odai, S. N. (2022). Evaluation of potential evapotranspiration assessment methods for hydrological modelling with SWAT in the Densu river basin in Ghana. *International Journal of Environmental Science and Technology*, 1-10.

Ahamed, A., Knight, R., Alam, S., Pauloo, R., & Melton, F. (2022). Assessing the utility of remote sensing data to accurately estimate changes in groundwater storage. *Science of The Total Environment*, *807*, 150635.

Althoff, D., Santos, R. A. D., Bazame, H. C., Cunha, F. F. D., & Filgueiras, R. (2019). Improvement of Hargreaves–Samani reference evapotranspiration estimates with local calibration. *Water*, *11*(11), 2272.

Anapalli, S. S., Fisher, D. K., Reddy, K. N., Wagle, P., Gowda, P. H., & Sui, R. (2018). Quantifying soybean evapotranspiration using an eddy covariance approach. *Agricultural Water Management*, *209*, 228-239.

Aouissi, J., Benabdallah, S., Chabaane, Z. L., & Cudennec, C. (2016). Evaluation of potential evapotranspiration assessment methods for hydrological modelling with SWAT—Application in data-scarce rural Tunisia. *Agricultural Water Management*, *174*, 39-51.

Arnold, J. G., Srinivasan, R., Muttiah, R. S., & Williams, J. R. (1998). Large area hydrologic modeling and assessment part I: model development 1. JAWRA Journal of the American Water Resources Association, 34(1), 73-89.

Baiamonte, G. (2019). SCS curve number and green-Ampt infiltration models. *Journal of Hydrologic Engineering*, *24*(10), 04019034.

Balathandayutham, K., &Valliammai, A. (2017). Analysis of rainfall parameters in Walayar watershed of Parambikulam-Aliyar-Palar basin, Coimbatore, Tamil Nadu. *Trends in Biosciences*, *10*(1), 152-158.

Balsamo, G., Albergel, C., Beljaars, A., Boussetta, S., Brun, E., Cloke, H., ...&Vitart, F. (2015). ERA-Interim/Land: a global land surface reanalysis data set. *Hydrology and Earth System Sciences*, *19*(1), 389-407.

Bao, X., & Zhang, F. (2013). Evaluation of NCEP–CFSR, NCEP–NCAR, ERA-Interim, and ERA-40 reanalysis datasets against independent sounding observations over the Tibetan Plateau. Journal of climate, 26(1), 206-214.

Bromwich, D. H., & Wang, S. H. (2005). Evaluation of the NCEP–NCAR and ECMWF 15-and 40-yr reanalyses using rawinsonde data from two independent Arctic field experiments. Monthly weather review, 133(12), 3562-3578.

Buttar, N. A., Yongguang, H., Shabbir, A., Lakhiar, I. A., Ullah, I., Ali, A., ...&Yasin, M. A. (2018). Estimation of evapotranspiration using Bowen ratio method. *IFAC-PapersOnLine*, *51*(17), 807-810.

Cantoni, E., Tramblay, Y., Grimaldi, S., Salamon, P., Dakhlaoui, H., Dezetter, A., &Thiemig, V. (2022). Hydrological performance of the ERA5 reanalysis for flood modeling in Tunisia with the LISFLOOD and GR4J models. *Journal of Hydrology: Regional Studies*, *42*, 101169.

Chejarla, V. R., Mandla, V. R., Palanisamy, G., &Choudhary, M. (2017). Estimation of damage to agriculture biomass due to Hudhud cyclone and carbon stock assessment in cyclone affected areas using Landsat-8. Geocarto international, 32(6), 589-602.

da Costa Faria Martins, S., dos Santos, M. A., Lyra, G. B., de Souza, J. L., Lyra, G. B., Teodoro, I., de Souza, R. C. (2022). Actual evapotranspiration for sugarcane based on Bowen ratio-energy balance and soil water balance models with optimized crop coefficients. Water Resources Management, 1-18. https://doi.org/10.1007/s11269-022-03263-5

Dahri, Z. H., Ludwig, F., Moors, E., Ahmad, S., Ahmad, B., Shoaib, M., ...&Kabat, P. (2021). Spatio-temporal evaluation of gridded precipitation products for the high-altitude Indus basin. *International Journal of Climatology*, *41*(8), 4283-4306.

Dallaire, G., Poulin, A., Arsenault, R., & Brissette, F. (2021). Uncertainty of potential evapotranspiration modelling in climate change impact studies on low flows in North America. *Hydrological Sciences Journal*, *66*(4), 689-702.

Das, S., &DSouza, N. M. (2020). Identifying the local factors of resilience during cyclone Hudhud and Phailin on the east coast of India. Ambio, 49(4), 950-961.

Dash, S. S., Sahoo, B., &Raghuwanshi, N. S. (2021). How reliable are the evapotranspiration estimates by Soil and Water Assessment Tool (SWAT) and

Variable Infiltration Capacity (VIC) models for catchment-scale drought assessment and irrigation planning?. *Journal of Hydrology*, *592*, 125838.

Dee, D. P., Uppala, S. M., Simmons, A. J., Berrisford, P., Poli, P., Kobayashi, S., ...&Vitart, F. (2011). The ERA-Interim reanalysis: Configuration and performance of the data assimilation system. Quarterly Journal of the royal meteorological society, 137(656), 553-597.

Degefu, M. A., Bewket, W., &Amha, Y. (2022). Evaluating performance of 20 global and quasi-global precipitation products in representing drought events in Ethiopia I: Visual and correlation analysis. *Weather and Climate Extremes*, *35*, 100416.

Desai, S., Singh, D. K., Islam, A., & Sarangi, A. (2021). Multi-site calibration of hydrological model and assessment of water balance in a semi-arid river basin of India. *Quaternary International*, *571*, 136-149.

Devia, G. K., Ganasri, B. P., &Dwarakish, G. S. (2015). A review on hydrological models. *Aquatic procedia*, *4*, 1001-1007.

Dile, Y. T., Ayana, E. K., Worqlul, A. W., Xie, H., Srinivasan, R., Lefore, N., ... & Clarke, N. (2020). Evaluating satellite-based evapotranspiration estimates for hydrological applications in data-scarce regions: A case in Ethiopia. Science of the Total Environment, 743, 140702.

Ebita, A., Kobayashi, S., Ota, Y., Moriya, M., Kumabe, R., Onogi, K., ...&Ishimizu, T. (2011). The Japanese 55-year reanalysis "JRA-55": an interim report. Sola, 7, 149-152.

Fennell, J., Soulsby, C., Wilkinson, M. E., Daalmans, R., & Geris, J. (2022). Assessing the role of location and scale of Nature Based Solutions for the enhancement of low flows. *International Journal of River Basin Management*, 1-16.

Ferreira, A. D. N., de Almeida, A., Koide, S., Minoti, R. T., &Siqueira, M. B. B. D. (2021). Evaluation of Evapotranspiration in Brazilian Cerrado Biome Simulated with the SWAT Model. *Water*, *13*(15), 2037.

Filgueiras, R., Venancio, L. P., Aleman, C. C., & da Cunha, F. F. (2022). Comparison and calibration of terraclimate climatological variables over the Brazilian territory. *Journal of South American Earth Sciences*, *117*, 103882.

Gavrilescu, M. (2021). Water, soil, and plants interactions in a threatened environment. *Water*, *13*(19), 2746.

Gebler, S., Hendricks Franssen, H. J., Pütz, T., Post, H., Schmidt, M., &Vereecken, H. (2015). Actual evapotranspiration and precipitation measured by lysimeters: a comparison with eddy covariance and tipping bucket. *Hydrology and earth system sciences*, *19*(5), 2145-2161.

Gehring, J., Duvvuri, B., &Beighley, E. (2022). Deriving River Discharge Using Remotely Sensed Water Surface Characteristics and Satellite Altimetry in the Mississippi River Basin. *Remote Sensing*, *14*(15), 3541.

Ghajarnia, N., Akbari, M., Saemian, P., Ehsani, M. R., Hosseini-Moghari, S. M., Azizian, A., ...&Haghighi, A. T. (2021). Evaluating the Evolution of ECMWF Precipitation Products Using Observational Data for Iran: From ERA40 to ERA5.

Ghonchepour, D., Sadoddin, A., Bahremand, A., Croke, B., Jakeman, A., &Salmanmahiny, A. (2021). A methodological framework for the hydrological model selection process in water resource management projects. *Natural Resource Modeling*, *34*(3), e12326

Gleason, C. J., Wada, Y., & Wang, J. (2018). A hybrid of optical remote sensing and hydrological modeling improves water balance estimation. *Journal of Advances in Modeling Earth Systems*, *10*(1), 2-17.

Gupta, A., Himanshu, S. K., Gupta, S., & Singh, R. (2020). Evaluation of the SWAT model for analysing the water balance components for the upper Sabarmati Basin. In *Advances in Water Resources Engineering and Management* (pp. 141-151). Springer, Singapore.

Hamal, K., Sharma, S., Khadka, N., Baniya, B., Ali, M., Shrestha, M. S., ...&Dawadi, B. (2020). Evaluation of MERRA-2 precipitation products using gauge observation in Nepal. *Hydrology*, *7*(3), 40.

Hargreaves, G. L., Hargreaves, G. H., & Riley, J. P. (1985). Agricultural benefits for Senegal River basin. Journal of irrigation and Drainage Engineering, 111(2), 113-124.

He, M., Kimball, J. S., Yi, Y., Running, S. W., Guan, K., Moreno, A., ... &Maneta, M. (2019). Satellite data-driven modeling of field scale evapotranspiration in croplands using the MOD16 algorithm framework. *Remote Sensing of Environment*, *230*, 111201.

Hersbach, H., Bell, B., Berrisford, P., Hirahara, S., Horányi, A., Muñoz-Sabater, J., ...&Thépaut, J. N. (2020). The ERA5 global reanalysis. Quarterly Journal of the Royal Meteorological Society, 146(730), 1999-2049.

Hirschi, M., Michel, D., Lehner, I., &Seneviratne, S. I. (2017). A site-level comparison of lysimeter and eddy covariance flux measurements of evapotranspiration. *Hydrology and Earth System Sciences*, *21*(3), 1809-1825.

Inayathulla, M. (2022). Application of a SWAT Model for Estimating Runoff and Other Hydrological Parameters in Cauvery River Sub-basins. In *Innovative Trends in Hydrological and Environmental Systems* (pp. 591-604). Springer, Singapore.

Jiang, Y., Wang, J., & Wang, Y. (2022). Daily Evapotranspiration Estimations by Direct Calculation and Temporal Upscaling Based on Field and MODIS Data. *Remote Sensing*, *14*(16), 4094.

Kalnay, E., Kanamitsu, M., Kistler, R., Collins, W., Deaven, D., Gandin, L., ...& Joseph, D. (1996). The NCEP/NCAR 40-year reanalysis project. Bulletin of the American meteorological Society, 77(3), 437-472.

Kamalanandhini, M., &Annadurai, R. (2022). Landuse and Land Cover Change Detection Using Geospatial Techniques for Drought Studies in Chengalpattu District,

Tamil Nadu, India. In Recent Developments in Sustainable Infrastructure (ICRDSI-2020)—GEO-TRA-ENV-WRM (pp. 563-570). Springer, Singapore.

Kanamitsu, M., Ebisuzaki, W., Woollen, J., Yang, S. K., Hnilo, J. J., Fiorino, M., & Potter, G. L. (2002). Ncep–doe amip-ii reanalysis (r-2). Bulletin of the American Meteorological Society, 83(11), 1631-1644.

Kayaba, N., Yamada, T., Hayashi, S., Onogi, K., Kobayashi, S., Yoshimoto, K., ...& Yamashita, K. (2016). Dynamical regional downscaling using the JRA-55 reanalysis (DSJRA-55). *Sola*, *12*, 1-5.

Kite, G. W., & Droogers, P. (2000). Comparing evapotranspiration estimates from satellites, hydrological models and field data. Journal of Hydrology, 229(1-2), 3-18.

Kobayashi, S., Ota, Y., Harada, Y., Ebita, A., Moriya, M., Onoda, H., ...& Takahashi, K. (2015). The JRA-55 reanalysis: General specifications and basic characteristics. *Journal of the Meteorological Society of Japan. Ser. II*, *93*(1), 5-48.

Kotal, S. D., Roy Bhowmik, S. K., Kundu, P. K., & Das Kumar, A. (2008). A statistical cyclone intensity prediction (SCIP) model for the Bay of Bengal. Journal of earth system science, 117(2), 157-168.

Kozlov, D., & Ghebrehiwot, A. (2022). Physically-Based Streamflow Predictions in Ungauged Basin with Semi-Arid Climate. In *Proceedings of FORM 2021* (pp. 549-565). Springer, Cham.

Krishna, P. R. (2019). Evapotranspiration and agriculture—A review. Agric. Rev, 40, 1-11.

Kumar, N., Dubey, A. K., Goswami, U. P., & Singh, S. K. (2022). Modelling of hydrological and environmental flow dynamics over a central Himalayan river basin through satellite altimetry and recent climate projections. *International Journal of Climatology*, 1– 26. https://doi.org/10.1002/joc.7734

Kumar, R., &Nandagiri, L. (2015, May). Application and Test of the SWAT Model in the Upper Cauvery River Basin, Karnataka, India. In *Proceedings of the 4th International Engineering Symposium Proceedings, Kumamoto, Japan* (pp. 23-24).

Landage, A. B., &Keshari, A. K. (2022). Swat Application for Water Balance Assessment of Koyna River Basin, Maharashtra, India. In *Hydrological Modeling* (pp. 97-107). Springer, Cham.

Lang, D., Zheng, J., Shi, J., Liao, F., Ma, X., Wang, W., ...& Zhang, M. (2017). A comparative study of potential evapotranspiration estimation by eight methods with FAO Penman–Monteith method in southwestern China. Water, 9(10), 734.

Li, D., Liang, Z., Zhou, Y., Li, B., & Fu, Y. (2019). Multicriteria assessment framework of flood events simulated with vertically mixed runoff model in semiarid catchments in the middle Yellow River. *Natural Hazards and Earth System Sciences*, *19*(9), 2027-2037.

Li, M., Zhang, P., & Han, J. (2022). Methods of Atmospheric Coherence Length Measurement. Applied Sciences, 12(6), 2980.

Li, W., Todorov, N., El-Askary, H. M., Piechota, T., &Struppa, D. (2020, December). Investigation of the Trends and Model Evaluations of multiple Hydrological Parameters over Global Arid Regions. In *AGU Fall Meeting Abstracts* (Vol. 2020, pp. H007-0002).

Li, Z., Zhang, Y., Wang, S., Yuan, G., Yang, Y., & Cao, M. (2010). Evapotranspiration of a tropical rain forest in Xishuangbanna, southwest China. Hydrological Processes, 24(17), 2405-2416.

Liang, X., Xie, Z., & Huang, M. (2003). A new parameterization for surface and groundwater interactions and its impact on water budgets with the variable infiltration capacity (VIC) land surface model. Journal of Geophysical Research: Atmospheres, 108(D16).

Lindsay, R., Wensnahan, M., Schweiger, A., & Zhang, J. (2014). Evaluation of seven different atmospheric reanalysis products in the Arctic. Journal of Climate, 27(7), 2588-2606.

Liu, L., Guo, Z., & Huang, G. (2018). Evaluation of water productivity under climate change in irrigated areas of the arid Northwest China using an assemble statistical downscaling method and an agro-hydrological model. *Proceedings of the International Association of Hydrological Sciences*, *379*, 393-402.

Long, D., Longuevergne, L., & Scanlon, B. R. (2014). Uncertainty in evapotranspiration from land surface modeling, remote sensing, and GRACE satellites. Water Resources Research, 50(2), 1131-1151.

Lu, H., Huang, W., Zeng, Y., Wang, P., Pi, X., & Liu, W. (2022). An unmixing-based spatial downscaling fusion approach for the MODIS evapotranspiration product. *Geocarto International*, 1-21.

Lu, J., Sun, G., McNulty, S. G., &Amatya, D. M. (2005). A comparison of six potential evapotranspiration methods for regional use in the southeastern United States 1. JAWRA Journal of the American Water Resources Association, 41(3), 621-633.

Ma, L., Zhang, T., Li, Q., Frauenfeld, O. W., & Qin, D. (2008). Evaluation of ERA-40, NCEP 1, and NCEP 2 reanalysis air temperatures with ground-based measurements in China. Journal of Geophysical Research: Atmospheres, 113(D15).

Mathew, M., Sreelash, K., Jacob, A. A., Mathew, M. M., &Padmalal, D. (2022). Diverging monthly rainfall trends in south peninsular India and their association with global climate indices. *Stochastic Environmental Research and Risk Assessment*, 1-22.

Mathison, C., Wiltshire, A. J., Falloon, P., &Challinor, A. J. (2015). South Asia river-flow projections and their implications for water resources. *Hydrology and Earth System Sciences*, *19*(12), 4783-4810.

McClean, F., Dawson, R., & Kilsby, C. (2021). Intercomparison of global reanalysis precipitation for flood risk modelling. *Hydrology and Earth System Sciences Discussions*, 1-13.

McNally, A. (2018). FLDAS noah land surface model L4 global monthly 0.1× 0.1

degree (MERRA-2 and CHIRPS). Atmos. Compos. Water Energy Cycles Clim. Var. https://disc.gsfc.nasa.gov/datasets/FLDAS_NOAH01_C_GL_M_001/summary

McNally, A. (2018). GES DISC Dataset: FLDAS Noah Land Surface Model L4 Global Monthly 0.1 0.1 degree (MERRA-2 and CHIRPS)(FLDAS_NOAH01_C_GL_M 001), NASA [data set].

McNally, A., Jung, H. C., Pervez, M. S., Shukla, S., Pricope, N. G., Harrison, L., & Peters-Lidard, C. D. (2016, December). Hydrologic Modeling for Monitoring Water Availability in Africa. In *AGU Fall Meeting Abstracts* (Vol. 2016, pp. H21E-1459).

McNally, A., Verdin, K., Harrison, L., Getirana, A., Jacob, J., Shukla, S., ...&Verdin, J. P. (2019). Acute water-scarcity monitoring for Africa. *Water*, *11*(10), 1968.

Meng, X., Ji, X., Liu, Z., Xiao, J., Chen, X., & Wang, F. (2014). Research on improvement and application of snowmelt module in SWAT. J. Nat. Resour, 29, 528-539.

Meng, X., Wang, H., Wu, Y., Long, A., Wang, J., Shi, C., & Ji, X. (2017). Investigating spatiotemporal changes of the land-surface processes in Xinjiang using high-resolution CLM3. 5 and CLDAS: Soil temperature. Scientific Reports, 7(1), 1-14.

Mengistu, A. G., Woldesenbet, T. A., &Dile, Y. T. (2022). Evaluation of observed and satellite-based climate products for hydrological simulation in data-scarce Baro-Akob River Basin, Ethiopia. *Ecohydrology& Hydrobiology*, *22*(2), 234-245.

Monteith, J. L. (1965). Evaporation and environment. In Symposia of the society for experimental biology (Vol. 19, pp. 205-234). Cambridge University Press (CUP) Cambridge.

Moorhead, J. E., Marek, G. W., Gowda, P. H., Lin, X., Colaizzi, P. D., Evett, S. R., &Kutikoff, S. (2019). Evaluation of evapotranspiration from eddy covariance using large weighing lysimeters. *Agronomy*, *9*(2), 99.

Muniandy, J. M., Yusop, Z., &Askari, M. (2016). Evaluation of reference evapotranspiration models and determination of crop coefficient for Momordicacharantia and Capsicum annuum. Agricultural Water Management, 169, 77-89.

Murty, P. L. N., Bhaskaran, P. K., Gayathri, R., Sahoo, B., Kumar, T. S., & SubbaReddy, B. (2016). Numerical study of coastal hydrodynamics using a coupled model for Hudhud cyclone in the Bay of Bengal. Estuarine, Coastal and Shelf Science, 183, 13-27.

Nadimpalli, R., Srivastava, A., Prasad, V. S., Osuri, K. K., Das, A. K., Mohanty, U. C., & Niyogi, D. (2020). Impact of INSAT-3D/3DR radiance data assimilation in predicting tropical cyclone Titli over the Bay of Bengal. IEEE Transactions on Geoscience and Remote Sensing, 58(10), 6945-6957.

Narayanan, M., &Venugopal, T. (2021). Identification of Groundwater Potential Zones using Geospatial Techniques in Palar River Basin, Tamil Nadu, India.

Naseef, T. M., & Kumar, V. S. (2020). Influence of tropical cyclones on the 100-year return period wave height—A study based on 39-year long ERA5 reanalysis data. International Journal of Climatology, 40(4), 2106-2116.

National Register of Large Dams (Status 1/2018)

Nigam, S., Ruiz-Barradas, A., &Sengupta, A. (2021). The Chennai Water Crisis: Insufficient rainwater or suboptimal harnessing of runoff?. Current science, 120(1), 43.

Nouri, M., &Homaee, M. (2022). Reference crop evapotranspiration for data-sparse regions using reanalysis products. *Agricultural Water Management*, *262*, 107319.

Ochege, F. U., Shi, H., Li, C., Ma, X., Igboeli, E. E., & Luo, G. (2021). Assessing Satellite, Land Surface Model and Reanalysis Evapotranspiration Products in the Absence of In-Situ in Central Asia. *Remote Sensing*, *13*(24), 5148.

Palar report (2015). National Water Mission. http://cgwb.gov.in/AQM/NAQUIM_REPORT/TAMILNADU/AQM%20Palar%20-%20final.pdf (Access date on: 26.09.2022)

Palar Intra-state Link Project of Tamil Nadu, chapter-3, National Water Development Agency

Pan, S., Xu, Y. P., Xuan, W., Gu, H., & Bai, Z. (2019). Appropriateness of potential evapotranspiration models for climate change impact analysis in YarlungZangbo River Basin, China. *Atmosphere*, *10*(8), 453.

Pandi, D., Kothandaraman, S., Kasiviswanathan, K. S., & Kuppusamy, M. (2022). A catchment scale assessment of water balance components: a case study of Chittar catchment in South India. *Environmental Science and Pollution Research*, 1-13.

Paparrizos, S., Maris, F., &Matzarakis, A. (2017). Sensitivity analysis and comparison of various potential evapotranspiration formulae for selected Greek areas with different climate conditions. Theoretical and Applied Climatology, 128(3), 745-759.

Parajuli, P. B., Risal, A., Ouyang, Y., & Thompson, A. (2022). Comparison of SWAT and MODIS Evapotranspiration Data for Multiple Timescales. *Hydrology*, *9*(6), 103.

Paul-Limoges, E., Wolf, S., Schneider, F. D., Longo, M., Moorcroft, P., Gharun, M., &Damm, A. (2020). Partitioning evapotranspiration with concurrent eddy covariance measurements in a mixed forest. *Agricultural and Forest Meteorology*, *280*, 107786.

Pavelsky, T. M., Durand, M. T., Andreadis, K. M., Beighley, R. E., Paiva, R. C., Allen, G. H., & Miller, Z. F. (2014). Assessing the potential global extent of SWOT river discharge observations. *Journal of Hydrology*, *519*, 1516-1525.

Pervez, M. S., McNally, A., & Shukla, S. (2016, December). Evaluation of Famine Early Warning Systems Network (FEWS NET) Land Data Assimilation System (FLDAS) and application in East Africa. In *AGU Fall Meeting Abstracts* (Vol. 2016, pp. H51I-1639).

Ponnurangam, G. G., Setiyono, T. D., Maunahan, A., Satapathy, S. S., Quicho, E., Gatti, L., ...&Holecz, F. (2019). quantitative assessment of rice crop damage post titli cyclone

inSrikakulam, Andhra Pradesh using geo-spatial techniques. International Archives of the Photogrammetry, Remote Sensing & Spatial Information Sciences.

Ramuje, K., & Rao, B. N. M. (2015). Hudhud cyclone—a severe disaster in Visakhapatnam. Int J Res EngTechnol, 3, 156-163.

Raza, A., Al-Ansari, N., Hu, Y., Acharki, S., Vishwakarma, D. K., Aghelpour, P., ...& Elbeltagi, A. (2022). Misconceptions of Reference and Potential Evapotranspiration: A PRISMA-Guided Comprehensive Review. *Hydrology*, *9*(9), 153.

Razavi, T., &Coulibaly, P. (2013). Streamflow prediction in ungauged basins: review of regionalization methods. *Journal of hydrologic engineering*, *18*(8), 958-975.

Raziei, T., &Parehkar, A. (2021). Performance evaluation of NCEP/NCAR reanalysis blended with observation-based datasets for estimating reference evapotranspiration across Iran. *Theoretical and Applied Climatology*, *144*(3), 885-903.

Refsgaard, J. C., Storm, B., & Clausen, T. (2010). SystèmeHydrologiqueEuropeén (SHE): review and perspectives after 30 years development in distributed physically-based hydrological modelling. *Hydrology Research*, *41*(5), 355.

Reichle, R. H., Draper, C. S., Liu, Q., Girotto, M., Mahanama, S. P., Koster, R. D., & De Lannoy, G. J. (2017). Assessment of MERRA-2 land surface hydrology estimates. *Journal of Climate*, *30*(8), 2937-2960.

Resmi, M. R., Achyuthan, H., & Jaiswal, M. K. (2017). Holocene tectonic uplift using geomorphometric parameters, GIS and OSL dating: Palar River basin, southern peninsular India. ZeitschriftfürGeomorphologie, 61(3), 243-265.

Resmi, MR., & Hema Achyuthan (2019). Quantitative analysis of the drainage and morphometric characteristics of the Palar River basin, Southern Peninsular India; using bAd calculator (bearing azimuth and drainage) and GIS. *Geology, Ecology, and Landscapes*, *3*(4), 295-307.

Rienecker, M. M., Suarez, M. J., Gelaro, R., Todling, R., Bacmeister, J., Liu, E., ...& Woollen, J. (2011). MERRA: NASA's modern-era retrospective analysis for research and applications. Journal of climate, 24(14), 3624-3648.

Roul, A. R., Pradhan, S. P., &Sahoo, K. C. (2022). Mass Movement and Initiation of Landslide Dam Burst in the Eastern Ghats, India during the Titli Cyclone. Journal of the Geological Society of India, 98(4), 538-544.

Saha, S., Moorthi, S., Pan, H. L., Wu, X., Wang, J., Nadiga, S., ...& Goldberg, M. (2010). The NCEP climate forecast system reanalysis. Bulletin of the American Meteorological Society, 91(8), 1015-1058.

Sakal, A., Ball, J., & van Kalken, T. (2018). Concept of the integrated hydrological ensemble prediction system applied for the Nattai River catchment, Australia. *Journal of Applied Water Engineering and Research*, *6*(2), 162-169.

Samain, B., &Pauwels, V. R. N. (2013). Impact of potential and (scintillometer-based) actual evapotranspiration estimates on the performance of a lumped rainfall–runoff

model. Hydrology and Earth System Sciences, 17(11), 4525-4540.

Santra Mitra, S., Santra, A., & Kumar, A. (2021). Catchment specific evaluation of Aphrodite's and TRMM derived gridded precipitation data products for predicting runoff in a semi gauged watershed of Tropical India. *Geocarto International*, *36*(11), 1292-1308.

Sao, D., Kato, T., Tu, L. H., Thouk, P., Fitriyah, A., & Oeurng, C. (2020). Evaluation of different objective functions used in the sufi-2 calibration process of swat-cup on water balance analysis: A case study of the Pursat river basin, Cambodia. *Water*, *12*(10), 2901.

Scherrer, S. C., Hirschi, M., Spirig, C., Maurer, F., &Kotlarski, S. (2022). Trends and drivers of recent summer drying in Switzerland. *Environmental Research Communications*, *4*(2), 025004.

Singh, D., Sharma, V., & Juyal, V. (2018). Performances of NCEP-NCAR and NCEP-DOE reanalysis data for winter seasonal mean air temperature and winter seasonal total precipitation amount over the Western Himalayas (WH). *Meteorology and Atmospheric Physics*, *130*(5), 517-527.

Singh, L., & Saravanan, S. (2022). Evaluation of various spatial rainfall datasets for streamflow simulation using SWAT model of Wunna basin, India. *International Journal of River Basin Management*, *20*(3), 389-398.

Singh, R. P., & Gupta, P. K. (2016, July). Development in remote sensing techniques for hydrological studies. In *Proc Indian NatnSciAcad* (Vol. 82, No. 3, pp. 773-786).

Smakhtin, V. Y. (2006). An assessment of environmental flow requirements of Indian river basins (Vol. 107). IWMI.

Solaiman, T. A., &Simonovic, S. P. (2010). National Centers for Environmental Prediction–National Center for Atmospheric Research (NCEP–NCAR) reanalyses data for hydrologic modelling on a basin scale. *Canadian Journal of Civil Engineering*, *37*(4), 611-623.

Solignac, P. A., Brut, A., Selves, J. L., Béteille, J. P., Gastellu-Etchegorry, J. P., Keravec, P., ... & Ceschia, E. (2009). Uncertainty analysis of computational methods for deriving sensible heat flux values from scintillometer measurements. Atmospheric Measurement Techniques, 2(2), 741-753.

Weiland, F. S., Tisseuil, C., Dürr, H. H., Vrac, M., & van Beek, L. P. H. (2011). Selecting the optimal method to calculate daily global reference potential evaporation from CFSR reanalysis data. Hydrol. Earth Syst. Sci. Discuss., 8, 7355–7398

Srivastava, P. K., Han, D., Rico Ramirez, M. A., & Islam, T. (2013). Comparative assessment of evapotranspiration derived from NCEP and ECMWF global datasets through Weather Research and Forecasting model. Atmospheric Science Letters, 14(2), 118-125.

Sulla-Menashe, D., & Friedl, M. A. (2018). User guide to collection 6 MODIS land cover (MCD12Q1 and MCD12C1) product. *USGS: Reston, VA, USA*, *1*, 18.

Tabari, H., Grismer, M. E., &Trajkovic, S. (2013). Comparative analysis of 31 reference evapotranspiration methods under humid conditions. Irrigation Science, 31(2), 107-117.

Tang, F. F., Xu, H. S., & Xu, Z. X. (2012). Model calibration and uncertainty analysis for runoff in the Chao River Basin using sequential uncertainty fitting. *Procedia Environmental Sciences*, *13*, 1760-1770.

Tesemma, Z. K., Wei, Y., Peel, M. C., & Western, A. W. (2015). The effect of year-to-year variability of leaf area index on Variable Infiltration Capacity model performance and simulation of runoff. *Advances in Water Resources*, *83*, 310-322.

Dayal, D., Pandey, A., Gupta, P., &Mahanandaiah, Y. (2022). *Applicability of VIC model for hydrological simulations over Upper Ganga Basin, India* (No. IAHS2022-332). Copernicus Meetings.

Trambauer, P., Dutra, E., Maskey, S., Werner, M., Pappenberger, F., Van Beek, L. P. H., &Uhlenbrook, S. (2014). Comparison of different evaporation estimates over the African continent. Hydrology and Earth System Sciences, 18(1), 193-212.

Uppala, S. M., Kållberg, P. W., Simmons, A. J., Andrae, U., Bechtold, V. D. C., Fiorino, M., ... & Woollen, J. (2005). The ERA-40 re-analysis. Quarterly Journal of the Royal Meteorological Society: A journal of the atmospheric sciences, applied meteorology and physical oceanography, 131(612), 2961-3012.

Van Kesteren, B., Beyrich, F., Hartogensis, O. K., &Braam, M. (2015). Long-term evaluation of the Scintec boundary-layer scintillometer and the Wageningen large-aperture scintillometer: implications for scintillometer users. Boundary-layer meteorology, 156(2), 303-323.

Vasantha Kumaran, T., Murali, O. M., & Rani Senthamarai, S. (2020). Chennai floods 2005, 2015: Vulnerability, risk and climate change. In Urban Health Risk and Resilience in Asian Cities (pp. 73-100). Springer, Singapore.

Venkata Rao, G., Venkata Reddy, K., & Sridhar, V. (2020). Sensitivity of Microphysical Schemes on the Simulation of Post-Monsoon Tropical Cyclones over the North Indian Ocean. Atmosphere, 11(12), 1297.

Visakh, S., Raju, P. V., Kulkarni, S. S., &Diwakar, P. G. (2019). Inter-comparison of water balance components of river basins draining into selected delta districts of Eastern India. *Science of The Total Environment*, *654*, 1258-1269.

Wang, K., & Dickinson, R. E. (2012). A review of global terrestrial evapotranspiration: Observation, modeling, climatology, and climatic variability. Reviews of Geophysics, 50(2).

Wanniarachchi, S., &Sarukkalige, R. (2022). A Review on Evapotranspiration Estimation in Agricultural Water Management: Past, Present, and Future. Hydrology, 9(7), 123.

Wanzala, M. A., Ficchi, A., Cloke, H. L., Stephens, E. M., Badjana, H. M., & Lavers, D. A. (2022). Assessment of global reanalysis precipitation for hydrological

modelling in data-scarce regions: A case study of Kenya. *Journal of Hydrology: Regional Studies*, *41*, 101105.

Widmoser, P., &Wohlfahrt, G. (2018). Attributing the energy imbalance by concurrent lysimeter and eddy covariance evapotranspiration measurements. *Agricultural and forest meteorology*, *263*, 287-291.

Wiwoho, B. S., &Astuti, I. S. (2022). Runoff observation in a tropical Brantas watershed as observed from long-term globally available TerraClimate data 2001–2020. *Geoenvironmental Disasters*, *9*(1), 1-18.

Xiang, K., Li, Y., Horton, R., & Feng, H. (2020). Similarity and difference of potential evapotranspiration and reference crop evapotranspiration–a review. *Agricultural Water Management*, *232*, 106043.

Xu, C. Y., & Chen, D. (2005). Comparison of seven models for estimation of evapotranspiration and groundwater recharge using lysimeter measurement data in Germany. Hydrological Processes: An International Journal, 19(18), 3717-3734.

Yassin, F., Razavi, S., Wong, J. S., Pietroniro, A., &Wheater, H. (2019). Hydrologic-Land Surface Modelling of a Complex System under Precipitation Uncertainty: A Case Study of the Saskatchewan River Basin, Canada. Hydrology and Earth System Sciences Discussions, 1-40.

Zhang, B., Kang, S., Li, F., & Zhang, L. (2008). Comparison of three evapotranspiration models to Bowen ratio-energy balance method for a vineyard in an arid desert region of northwest China. Agricultural and forest meteorology, 148(10), 1629-1640.

Zhang, J., & Han, D. (2017). Catchment morphing (CM): a novel approach for runoff modeling in ungauged catchments. *Water Resources Research*, *53*(12), 10899-10907.

Zhang, K., Kimball, J. S., & Running, S. W. (2016). A review of remote sensing based actual evapotranspiration estimation. Wiley Interdisciplinary Reviews: Water, 3(6), 834-853.

Zhang, K., Kimball, J. S., & Running, S. W. (2016). A review of remote sensing based actual evapotranspiration estimation. *Wiley Interdisciplinary Reviews: Water*, *3*(6), 834-853.

Zhang, Y., Kong, D., Gan, R., Chiew, F. H., McVicar, T. R., Zhang, Q., & Yang, Y. (2019). Coupled estimation of 500 m and 8-day resolution global evapotranspiration and gross primary production in 2002–2017. *Remote sensing of environment*, *222*, 165-182.

Zhao, L., Xia, J., Xu, C. Y., Wang, Z., Sobkowiak, L., & Long, C. (2013). Evapotranspiration estimation methods in hydrological models. Journal of Geographical Sciences, 23(2), 359-369.

Zolina, O., Dufour, A., Gulev, S. K., &Stenchikov, G. (2017). Regional hydrological cycle over the Red Sea in ERA-Interim. *Journal of Hydrometeorology*, *18*(1), 65-83.

Gunnell, Y. (1997). Relief and climate in South Asia: the influence of the Western Ghats on the current climate pattern of peninsular India. International journal of climatology: a journal of the Royal Meteorological Society, 17(11), 1169-1182.

Resmi, M. R., Babeesh, C., & Achyuthan, H. (2019). Quantitative analysis of the drainage and morphometric characteristics of the Palar River basin, Southern Peninsular India; using bAd calculator (bearing azimuth and drainage) and GIS. Geology, ecology, and landscapes, 3(4).

Ramasamy, S., & Varghese, N. M. (2018). Provenance of the Gondwana sediments, Palar Basin, Southern India. Arabian Journal of Geosciences, 11, 1-18.

Dutta, S. K., & Prasad, V. S. (2010). Assessment of WRF-Var assimilation for a cyclonic storm–Nisha. Current Science, 86-91.

Balachandran, S., & Geetha, B. (2014). Characterisation and asymmetry analysis of rainfall distribution associated with tropical cyclones over Bay of Bengal: NISHA (2008), LAILA (2010) and JAL (2010). Mausam, 65(4), 481-496.

Srivastava, K., Bhardwaj, R., & Roy Bhowmik, S. K. (2011). Assimilation of Indian Doppler Weather Radar observations for simulation of mesoscale features of a land-falling cyclone. Natural Hazards, 59, 1339-1355.

Elnashar, A., Wang, L., Wu, B., Zhu, W., & Zeng, H. (2021). Synthesis of global actual evapotranspiration from 1982 to 2019. Earth System Science Data, 13(2), 447-480.

Singh, V. K., Pandey, H. K., & Singh, S. K. (2023a). Groundwater storage change estimation using GRACE data and Google Earth Engine: A basin scale study. Physics and Chemistry of the Earth, Parts A/B/C, 129, 103297.

Singh, V. K., Pandey, H. K., Singh, S. K., & Soni, P. (2023b). Groundwater analysis using Gravity Recovery, Climate Experiment and Google Earth Engine: Bundelkhand region, India. Physics and Chemistry of the Earth, Parts A/B/C, 130, 103401.

Rawat, K. S., Bala, A., Singh, S. K., & Pal, R. K. (2017). Quantification of wheat crop evapotranspiration and mapping: A case study from Bhiwani District of Haryana, India. Agricultural water management, 187, 200-209.

Rawat, K. S., Singh, S. K., Bala, A., & Szabó, S. (2019). Estimation of crop evapotranspiration through spatial distributed crop coefficient in a semi-arid environment. Agricultural Water Management, 213, 922-933.

Kushwaha, A. P., Tiwari, A. D., Dangar, S., Shah, H., Mahto, S. S., & Mishra, V. (2021). Multimodel assessment of water budget in Indian sub-continental river basins. Journal of Hydrology, 603, 126977.

Ansari, R., Liaqat, M. U., & Grossi, G. (2022). Evaluation of gridded datasets for terrestrial water budget assessment in the Upper Jhelum River Basin-South Asia. Journal of Hydrology, 613, 128294.

List of Tables

Table 1: Description of spatial datasets used for the PRB.

S. no	Spatial Data	Description	Source
1	Digital Elevation Model (DEM)	30 m×30 m grid DEM for delineation the watershed and analyze the drainage patterns of the terrain	Shuttle Radar Topography Mission (SRTM) of USGS (http://srtm.csi.cgiar.org/)
2	Land use and land cover (LULC)	Type1 at 500m resolution	MODIS Land Cover- Product MCD12Q1 (LP DAAC - MCD12Q1 (usgs.gov)
3	Soil data	The soil data has been obtained from FAO	FAO (Food and Agricultural Organization of the United Nations)(http://www.fao.org/soils-portal/soil-survey/soil-maps-anddatabases/en/, n.d.)
4	Weather data	ERA5 reanalysis dataset at 0.25° spatial resolution used	https://www.ecmwf.int/en/forecasts/datasets/reanalysis-datasets/era5
5	Hydrological data	Hydrological data (Discharge)	Gauge data at Chengalpattu gauge Station from Central Water Commission (CWC) Ministry of Water Resources, Government of India

Table 2: Description of spatial datasets used for comparative analysis at the PRB

		FLDAS Global model ET	FLDAS (Famine Early Warning Systems Network (FEWS

1	Evapotranspiration (ET) data	MOD16 global ET	NET) Land Data Assimilation System) https://ldas.gsfc.nasa.gov/fldas#
			https://modis.gsfc.nasa.gov/data/dataprod/mod16.php
		TerraClimate ET	https://www.climatologylab.org/terraclimate.html
2	Potential Evapotranspiration (PET) data	ERA5 Reanalysis Hargreaves PET	https://www.ecmwf.int/en/forecasts/datasets/reanalysis-datasets/era5
		TerraClimate PET	https://www.climatologylab.org/terraclimate.html
		MERRA2 PET	https://gmao.gsfc.nasa.gov/reanalysis/MERRA-2/data_access/
3	Surface runoff data	FLDAS	FLDAS (Famine Early Warning Systems Network (FEWS NET) Land Data Assimilation System)
		TerraClimate	https://www.climatologylab.org/terraclimate.html

1426

1427

1428 **Table 3:** Description of sensitive parameters for the PRB.

Parameter Name	Description	Rank	t-Stat	P-Value	Fitted Value	New minimum	New Maximum

V__GW_DELAY.gw	Groundwater delay (days).	1	2.16	0.6	17.23	16.68	17.78
r__CN2.mgt	runoff curve number	2	-7.77	0.0	-0.1	-0.156	-0.04
V__SLSUBBSN.hru	Average slope length.	3	0.76	0.46	149.62	149.3	149.95
r__SOL_Z(..).sol	Depth from soil surface to bottom of layer.	4	-0.61	0.55	0.12	0.03	0.21
V__RES_PSA.res	Reservoir surface area when the reservoir is filled to the principal spillway.	5	-2.33	0.04	233.75	216.18	251.32
V__RES_VOL.res	Initial reservoir volume.	6	0.26	0.79	83.75	66.09	101.4
V__RES_PVOL.res	Volume of water needed to fill the reservoir to the principal spillway.	7	-1.64	0.13	2987.5	2733.59	3241.41
V__ALPHA_BF.gw	Baseflow alpha factor (days)	8	0.53	0.61	0.04	0.02	0.06
r__HRU_SLP.hru	Average slope steepness	9	1.02	0.33	-0.27	-0.41	-0.13

1429

1430

1431 **Table 4:** SWAT calibration and validation result

Process	p-factor	r-factor	R^2	NSE	PBIAS
calibration	0.55	0.50	0.71	0.69	19.1
validation	0.47	0.52	0.65	0.63	-27.5

1432

1433

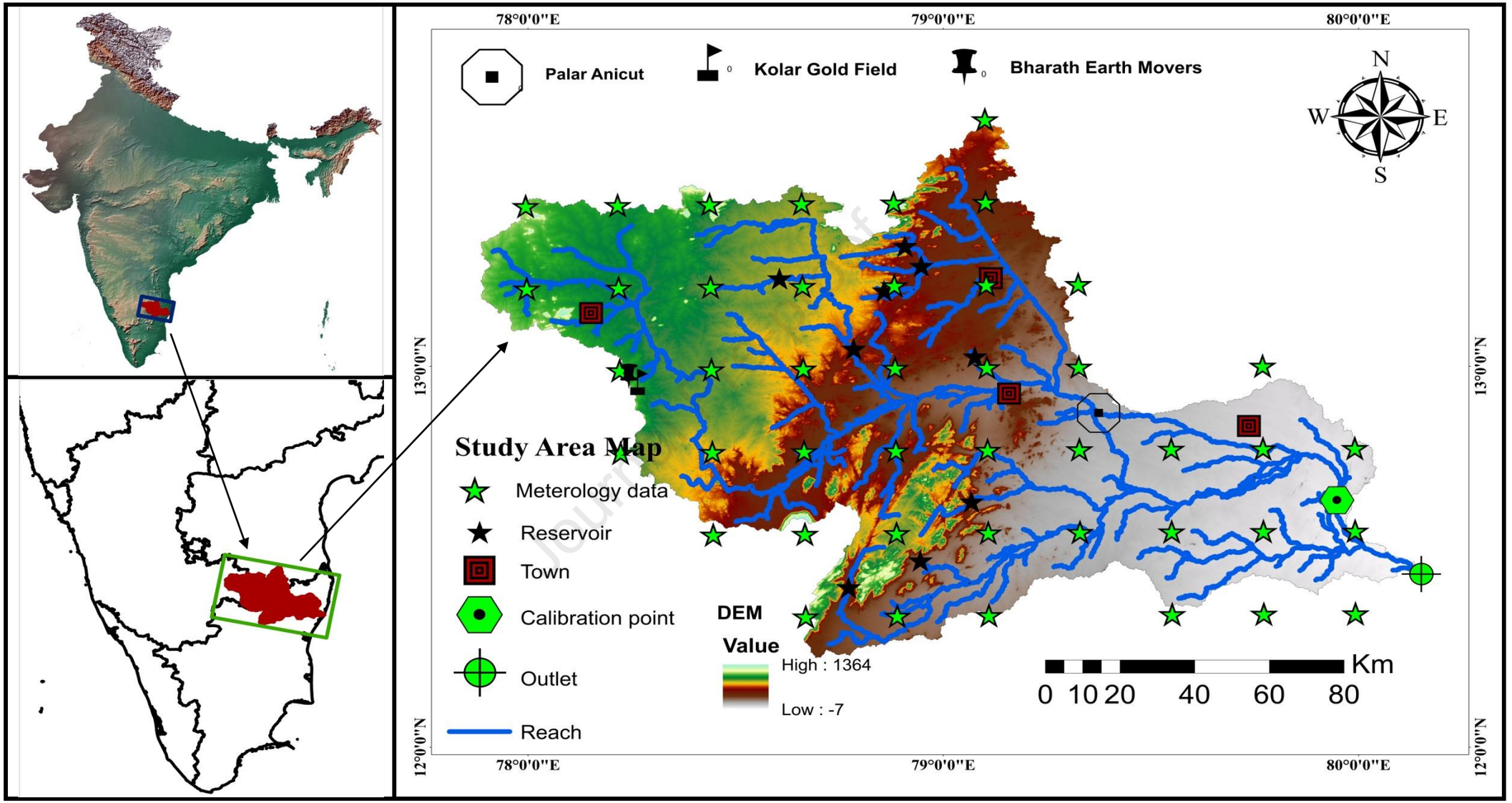

Fig. 1 The location map of the study region with meteorological stations, reservoirs, outlet and calibration point of the PRB.

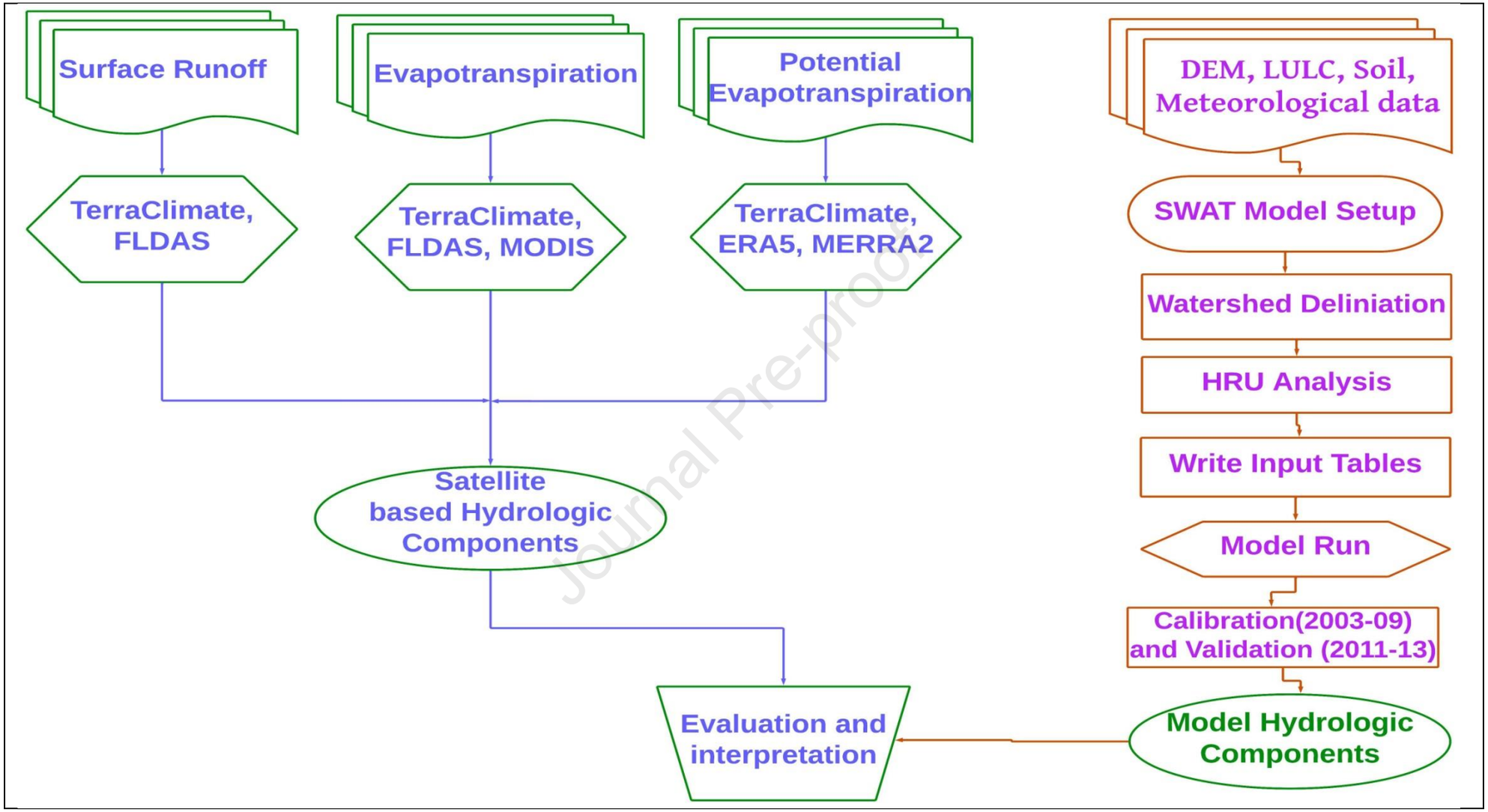

Fig. 2 The detailed methodology used in the quantitative estimation of water balance components in the PRB using the SWAT model and multi-satellite data.

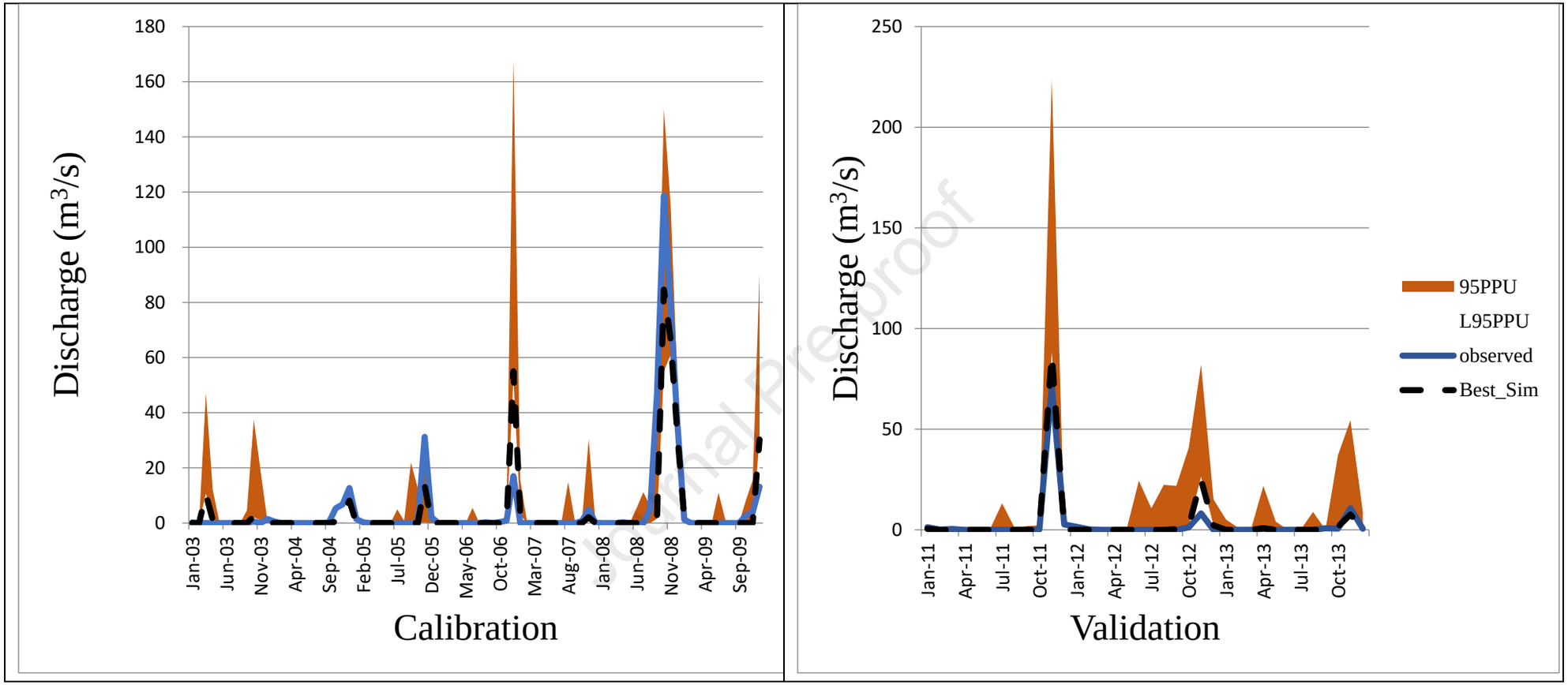

Fig. 3 The model performance evaluation of the SWAT model depicts the model efficiency as satisfactory to good during the calibration (2003-2009) and validation (2011-2013) period.

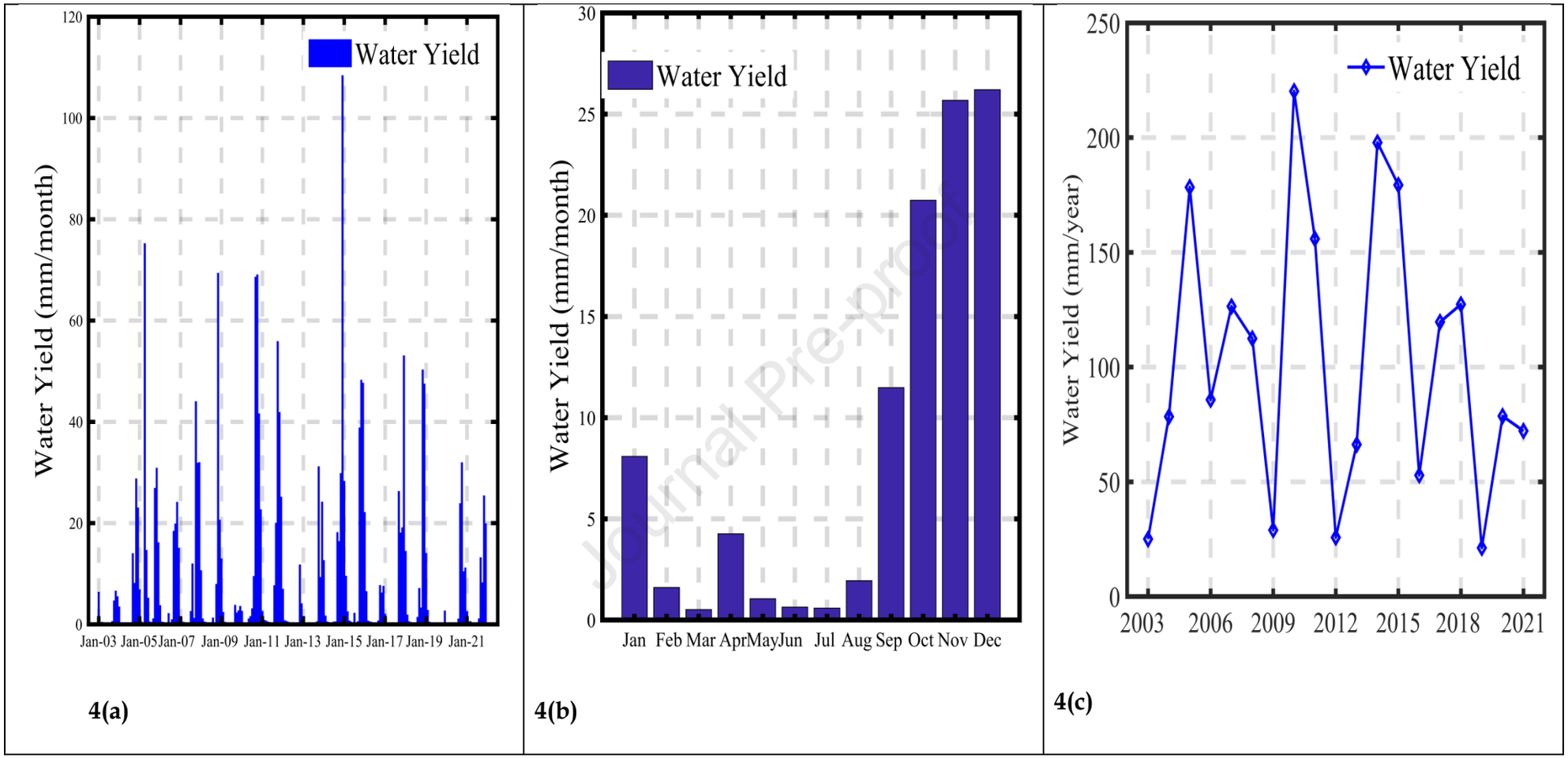

Fig. 4 Time series of (a) water yield (mm/month), (b) monthly water yield, and (c) SWAT simulated annual water yield at the calibration station of the basin (2003–2021).

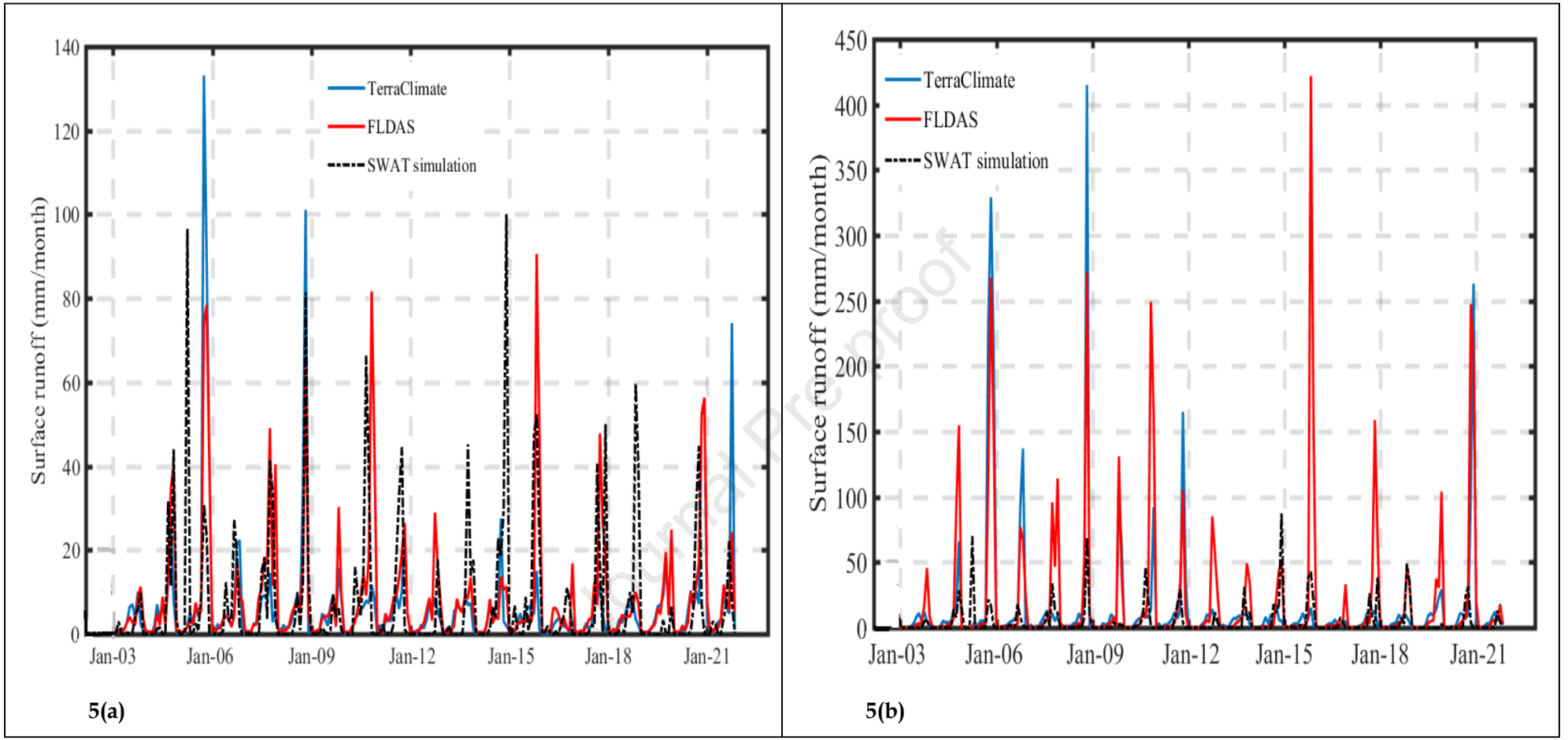

Fig.5(a) Comparison of monthly runoff from SWAT and freely accessible remote sensing data sets over the entire basin, (b) at the calibration station.

.

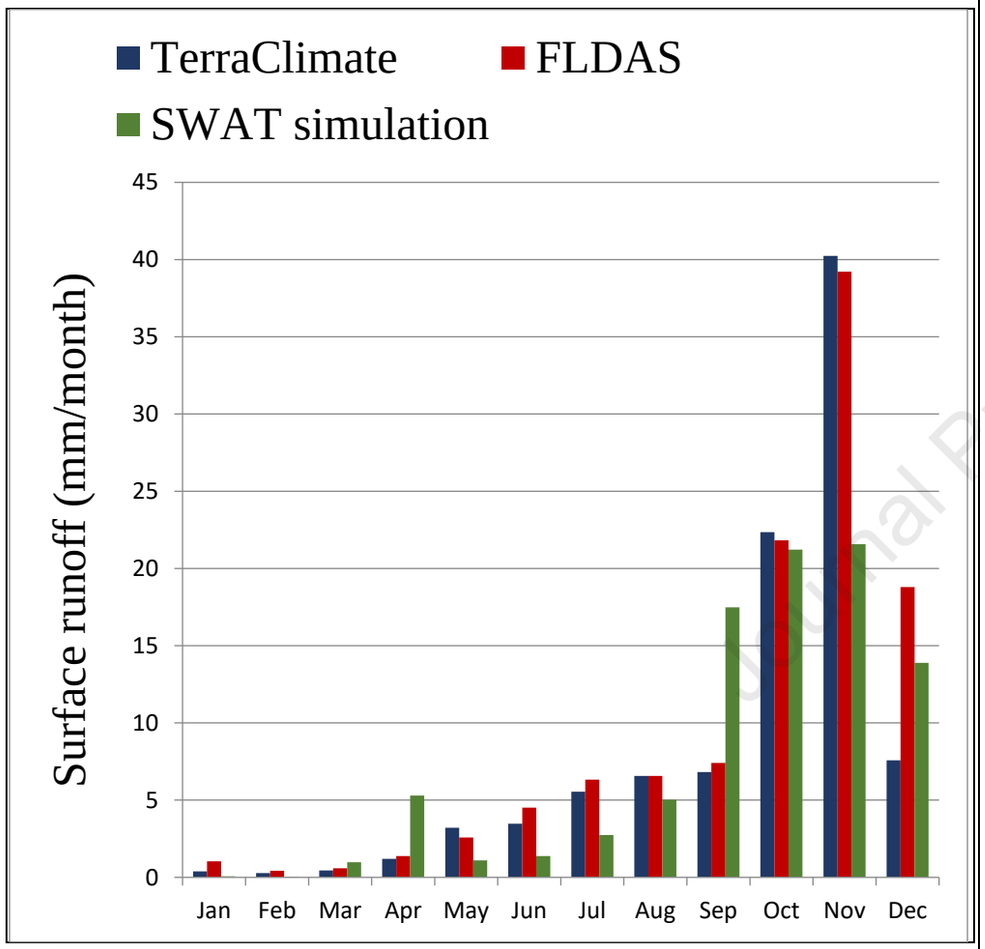

6(a)

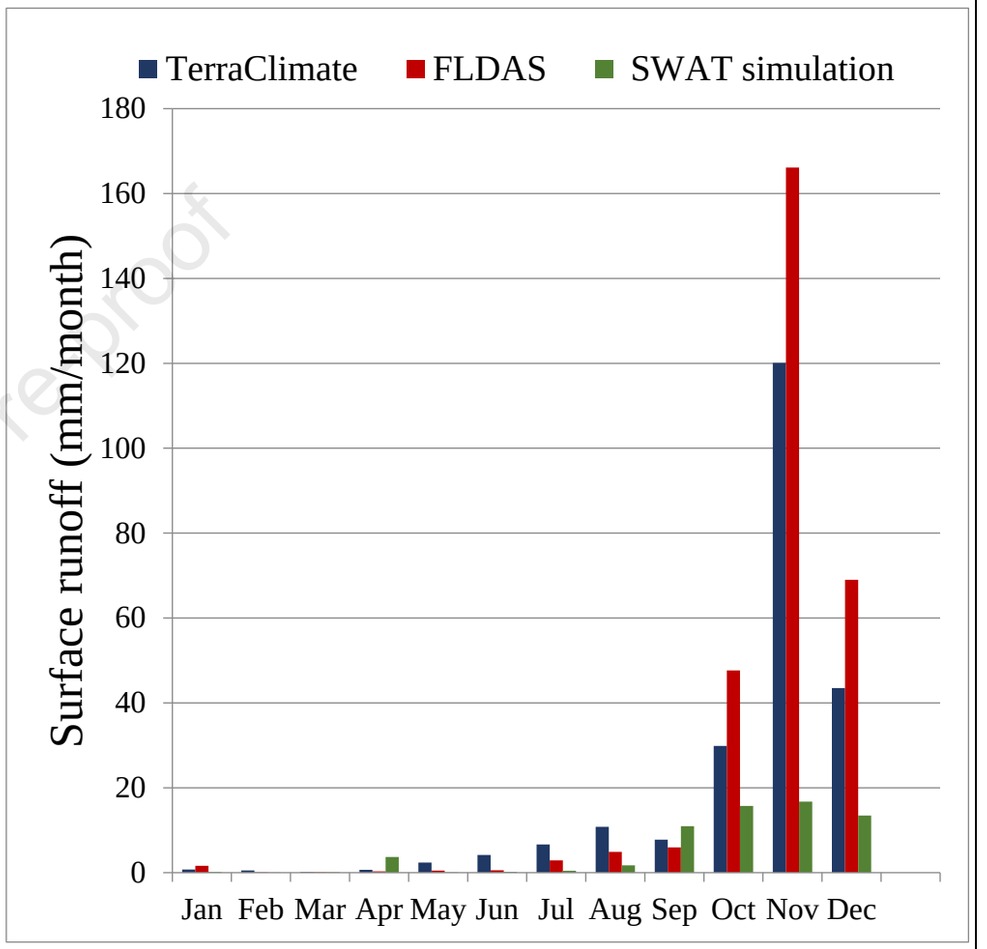

6(b)

Fig. 6(a) Comparison of the SWAT simulated monthly runoff with freely accessible remote sensing data-sets over the entire basin, and (b) at the calibration station.

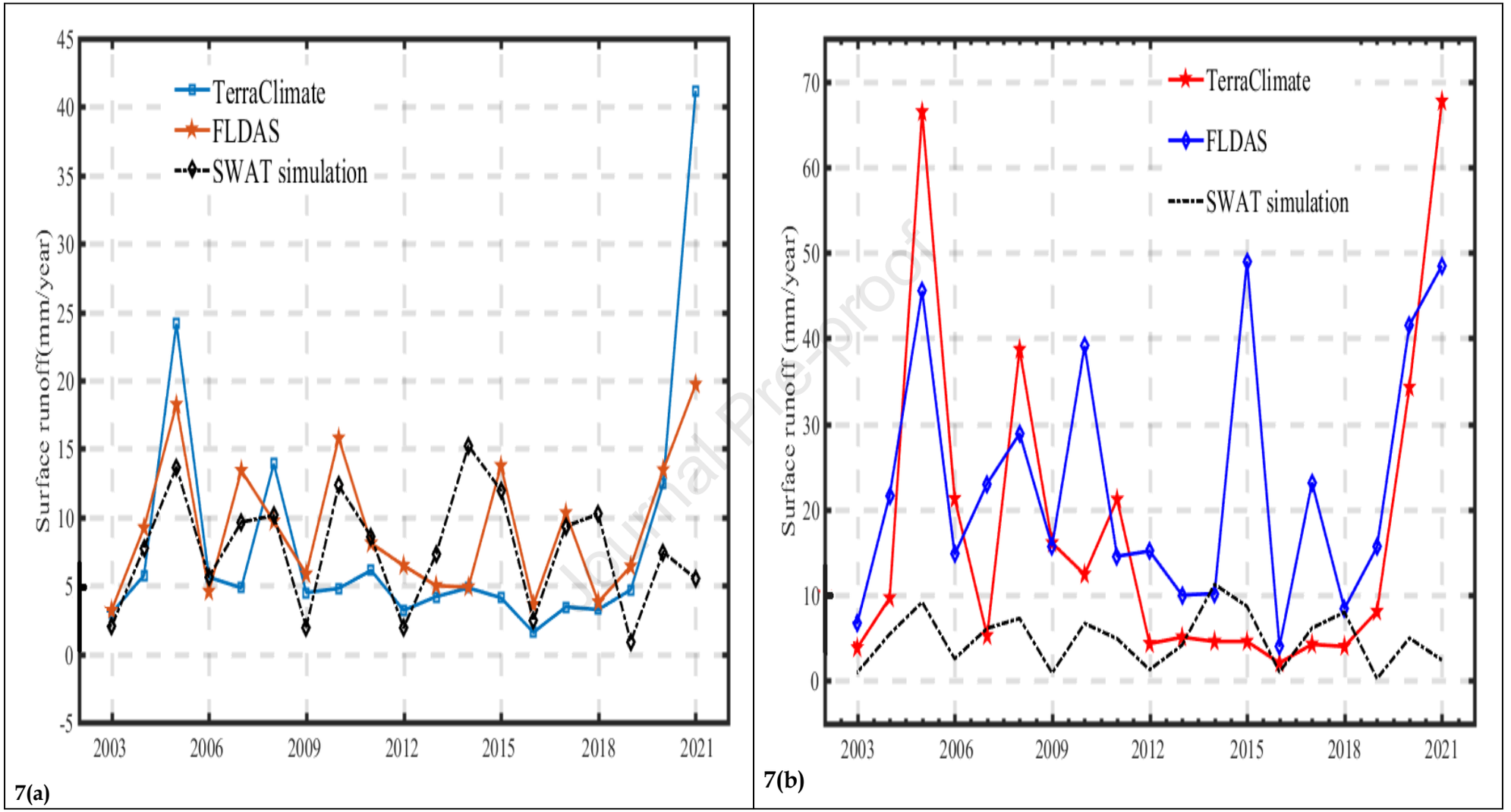

Fig. 7(a) Comparison of the SWAT simulated time series plot of runoff with freely accessible remote sensing data sets over the entire basin, and (b) at the calibration station.

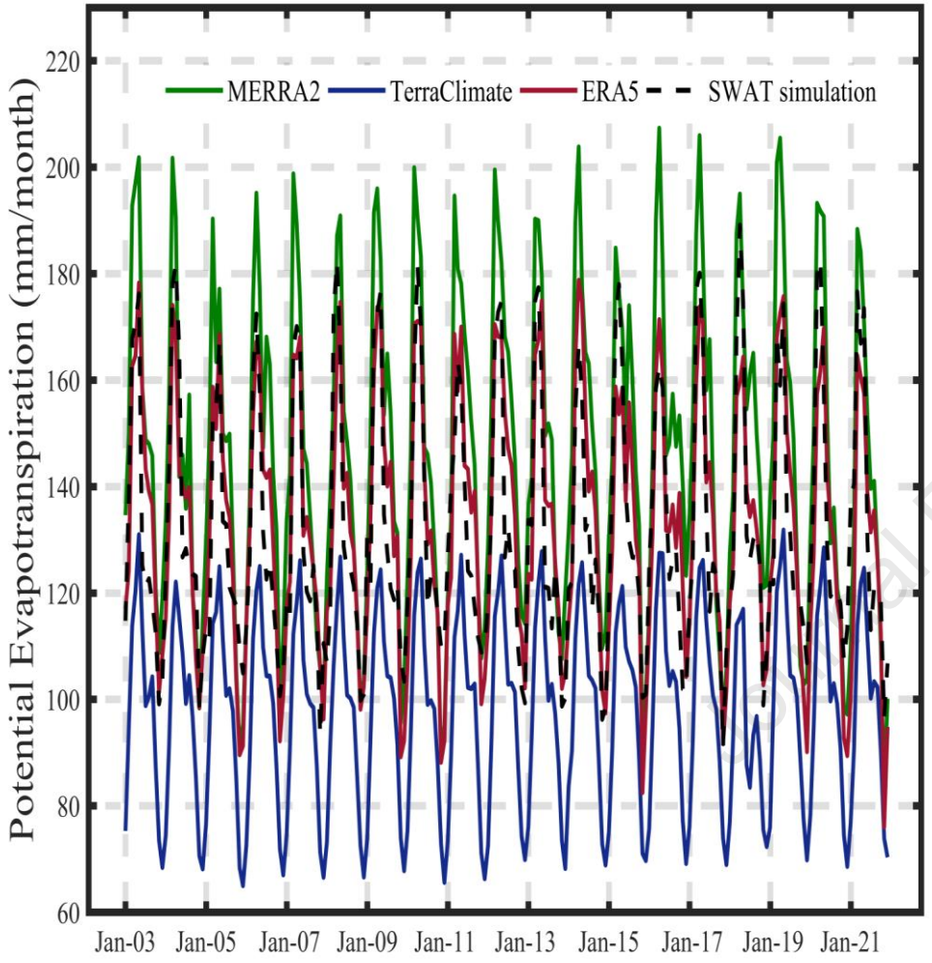

8(a)

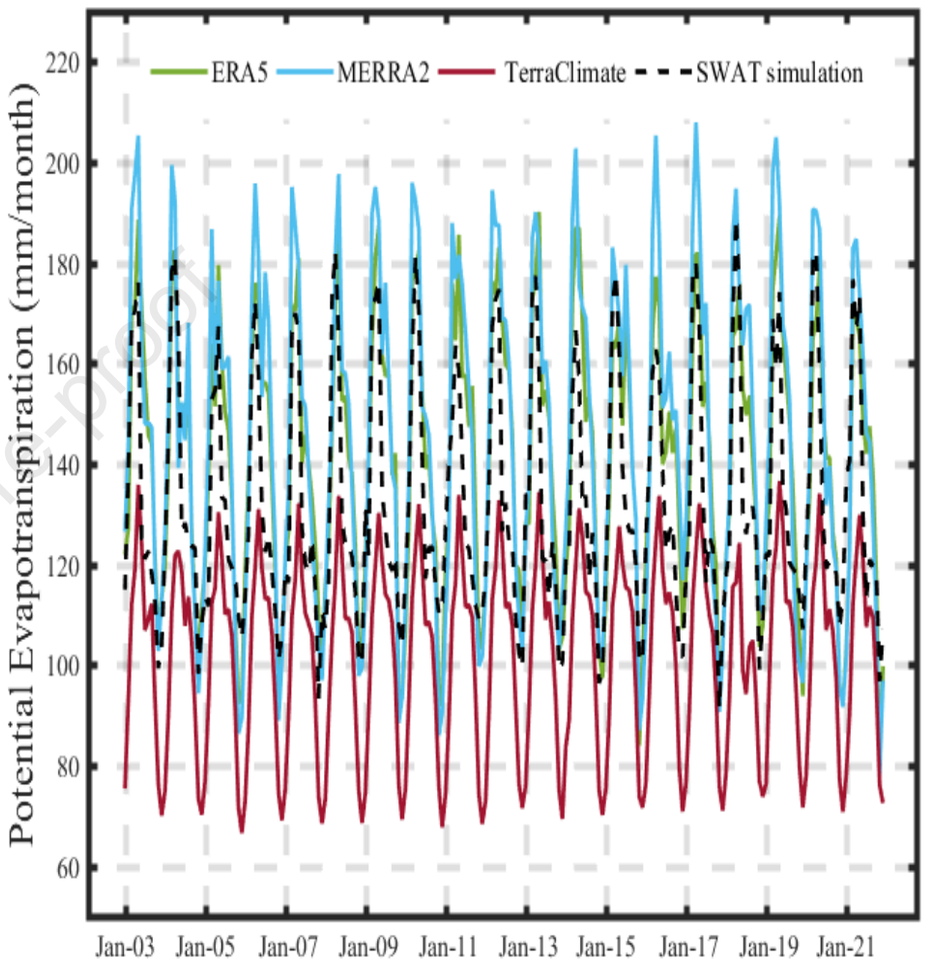

8(b)

Fig.8(a) Comparison of the SWAT simulated time series plot of PET with freely accessible remote sensing data sets over the entire basin, and (b) at the calibration station.

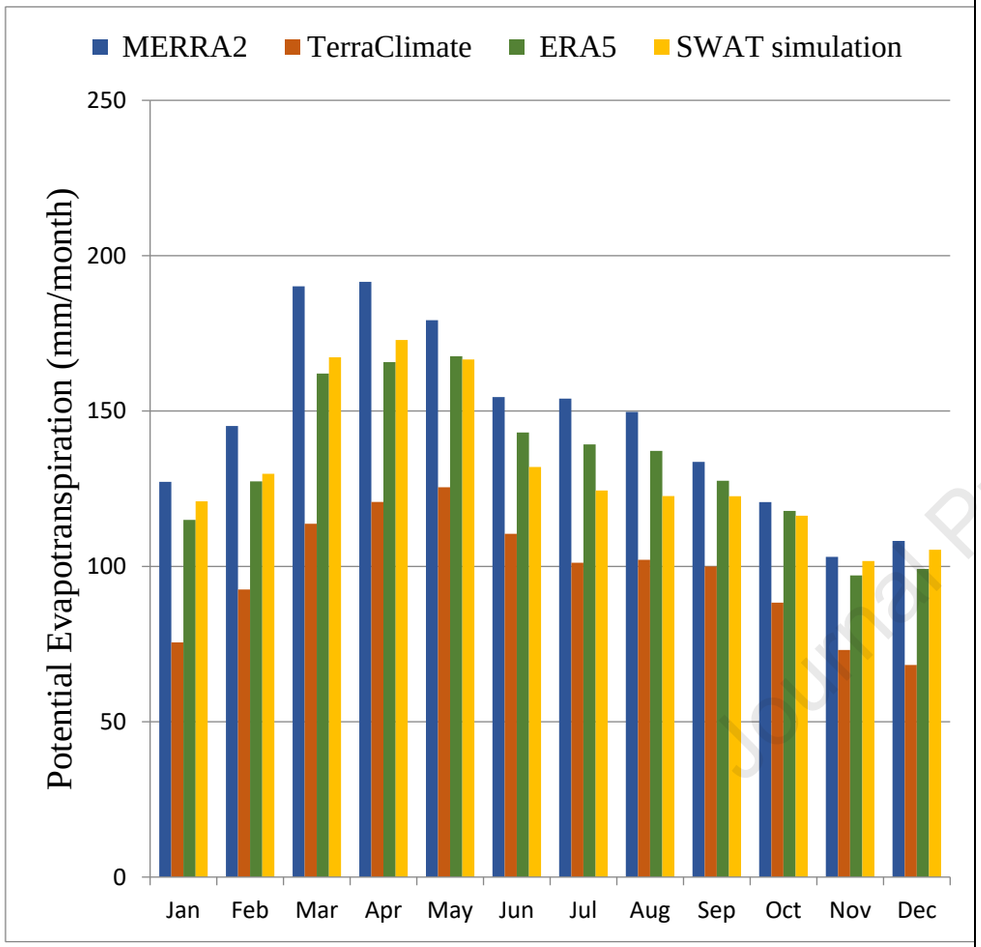

9(a)

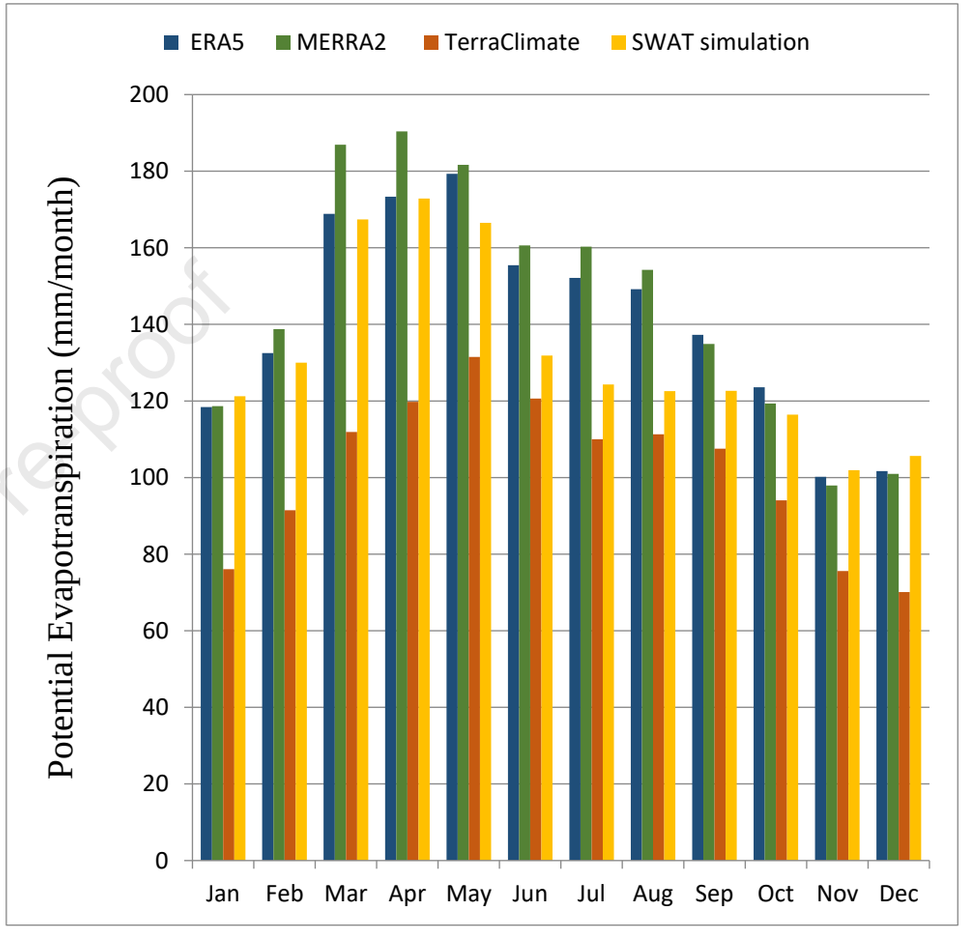

9(b)

Fig.9(a) Comparison of the monthly PET from SWAT simulation and freely accessible remote sensing data sets over the entire basin, and (b) at the calibration station.

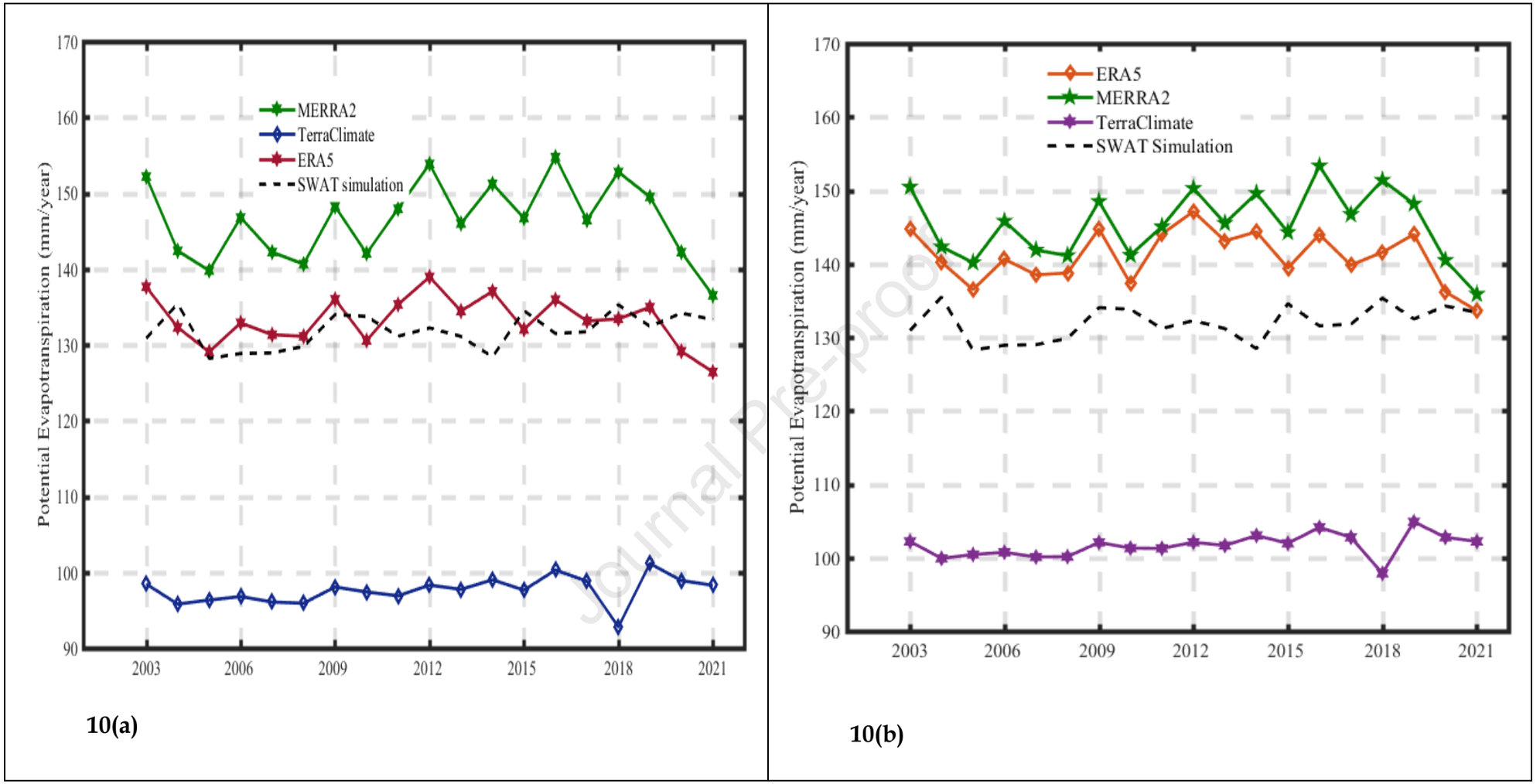

Fig. 10(a) comparison of the annual time series plot of Potential Evapotranspiration of SWAT simulated with freely accessible remote sensing data sets over the entire basin and (b) at the calibration station

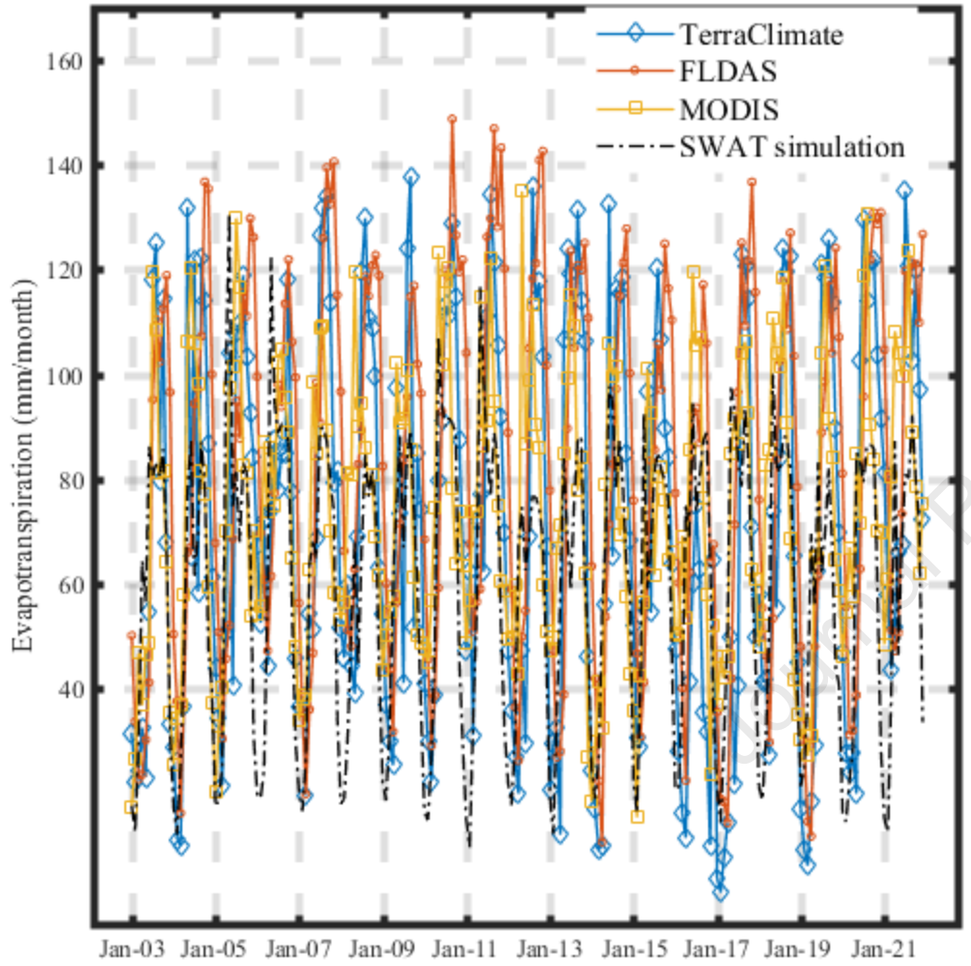

11(a)

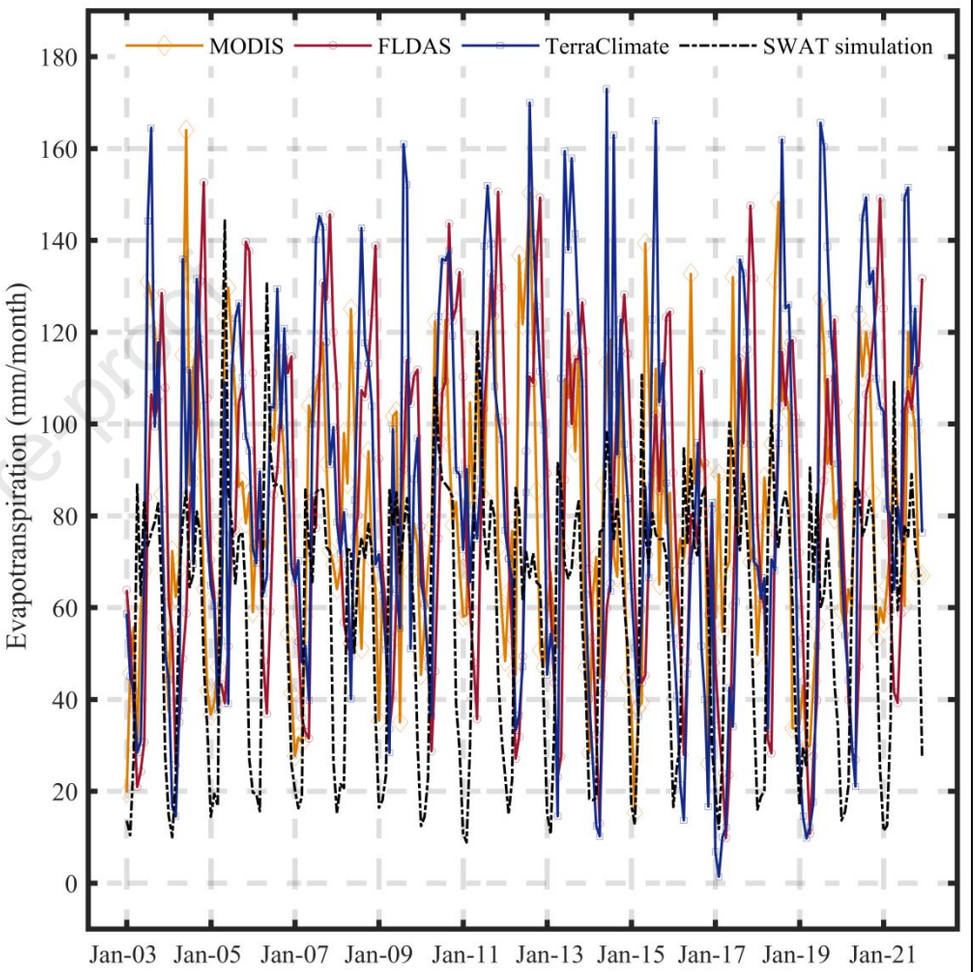

11(b)

Fig.11(a) comparison of the time series plot of the evapotranspirtion of SWAT simulation with freely accessible remote sensing data sets over the entire basin, and (b) at the calibration station

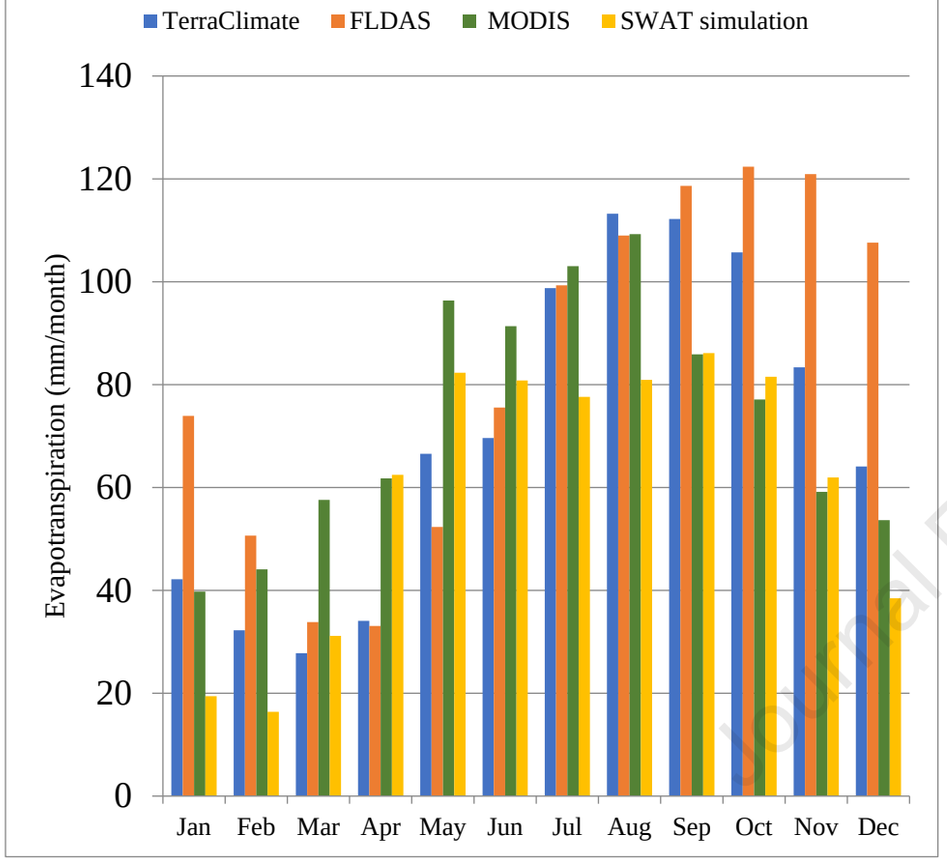

12(a)

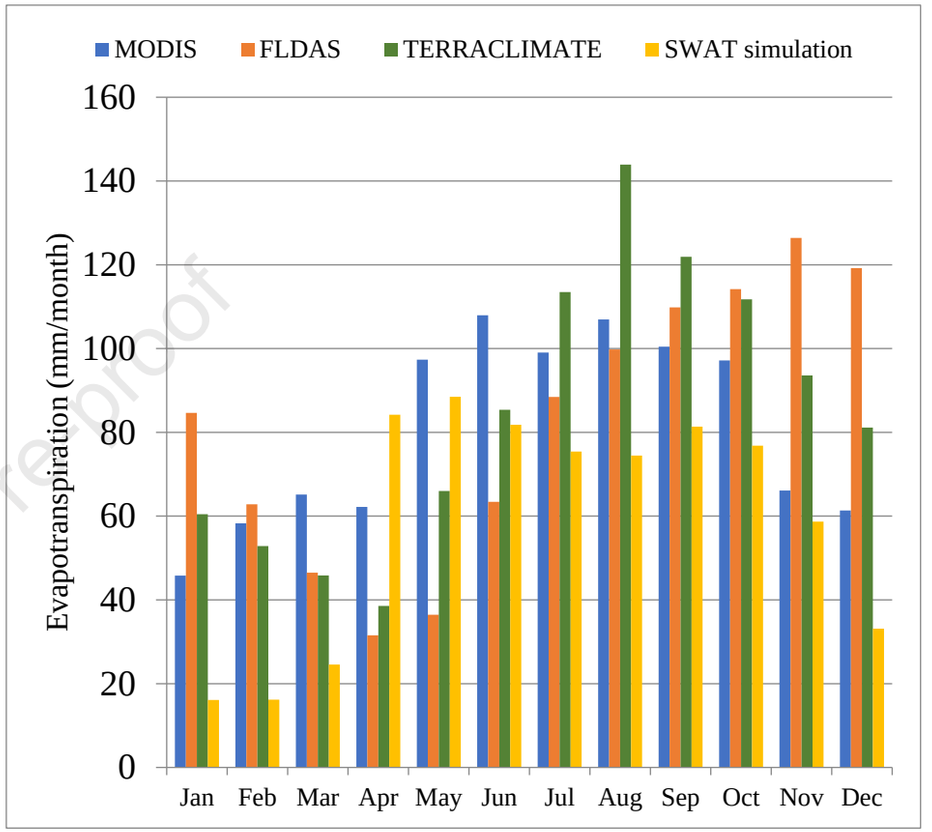

12(b)

Fig.12(a) The comparison of the monthly plot of Evapotraspirtion of SWAT simulated and freely accessible remote sensing data-sets over the entire basin, and (b) at the calibration station.

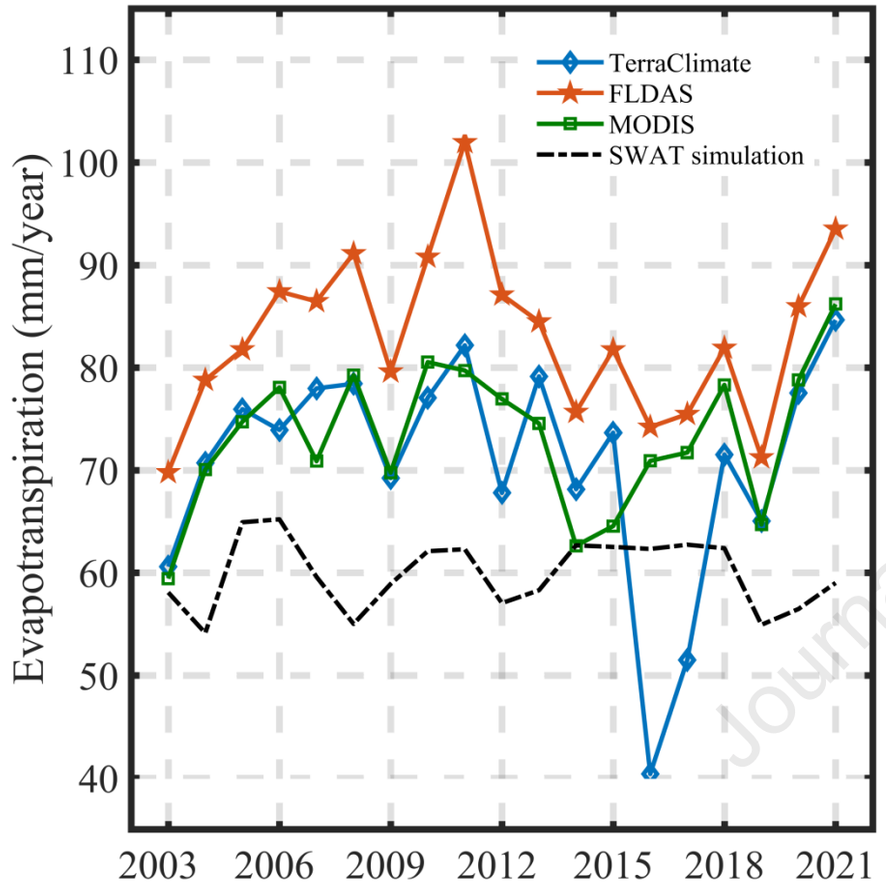

13(a)

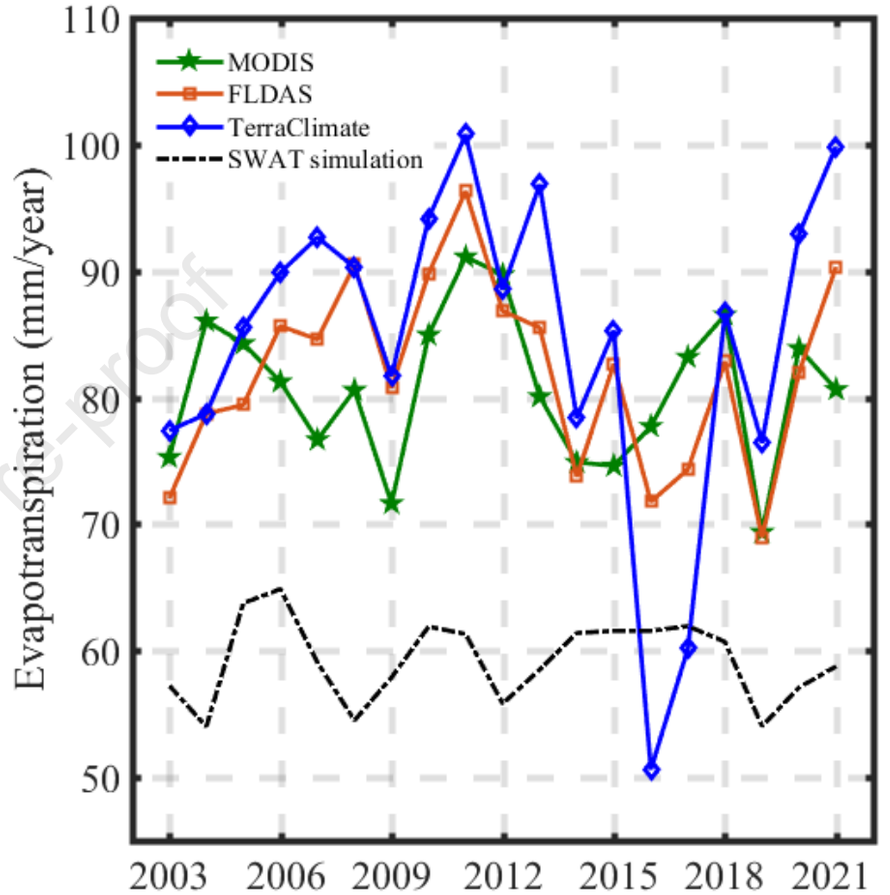

13(b)

Fig.13(a) The comparison of the annual time series plot of Evapotraspirtion of SWAT simulation with freely accessible remote sensing data-sets over the entire basin, and (b) at the calibration station(2003–2021).

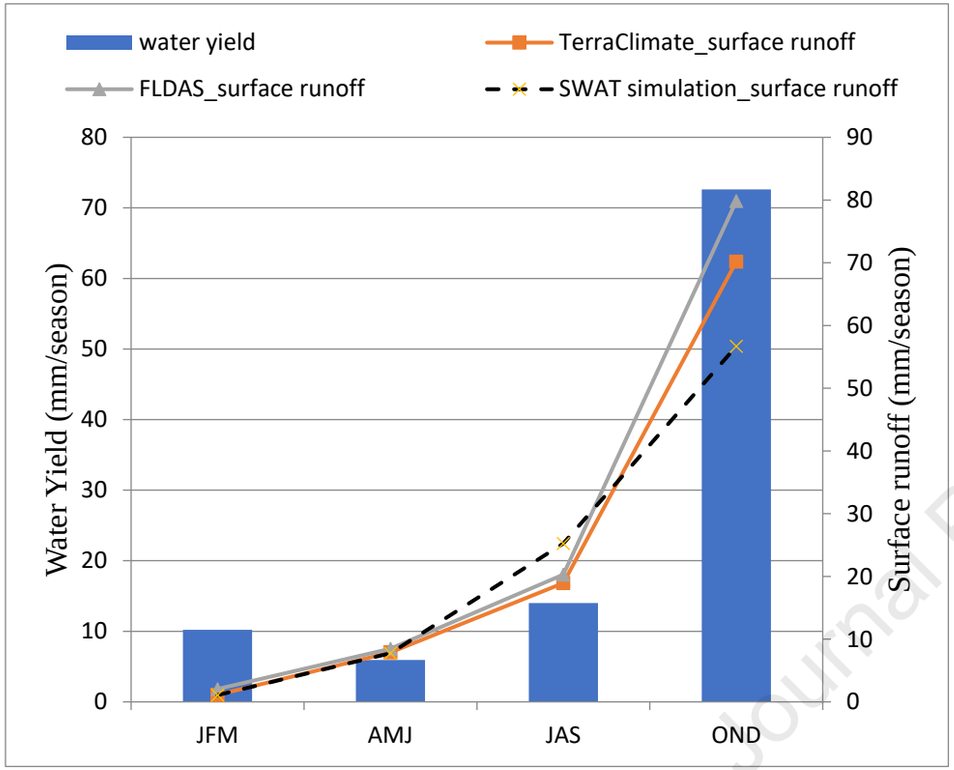

14(a)

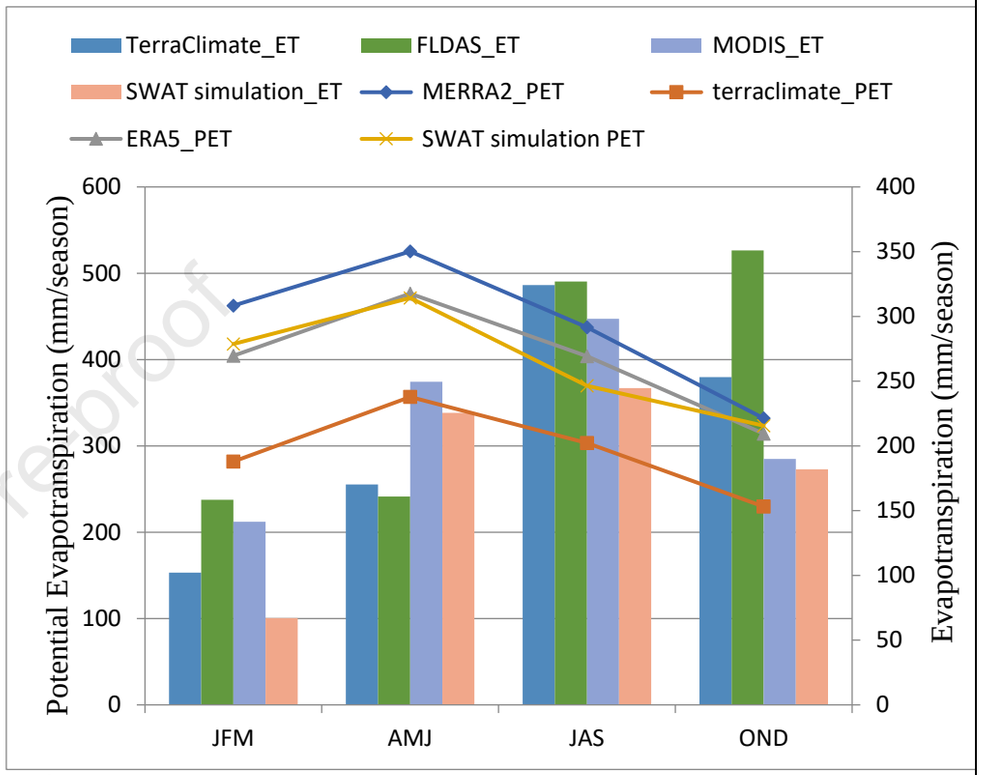

14(b)

Fig.14(a) representation of long –term average seasonal water yield, surface runoff, Evapotraspirtion and Potential Evapotraspirtion for the basin.

Highlights

- TerraClimate, FLDAS, MODIS, ERA5, & MERRA2 (PET) used for analysis
- Multi-satellite data were evaluated for poorly gauged river using SWAT
- Monthly, seasonal, & annual analysis was performed at basin & Chengalpattu
- Total average annual water yield for the entire basin was reported
- FLDAS & TerraClimate over predicted monthly surface runoff at Chengalpattu

Authors Statement

For research articles with several authors, a short paragraph specifying their individual contributions must be provided. The following statements should be used "Conceptualization, A.R.M., K.S.R, N.K, and S.K.S; methodology, A.R.M., K.S.R, N.K, and S.K.S.; software, A.R.M., K.S.R, N.K, P.K.S., S.Z. and S.K.S; validation, A.R.M., S.Z. and S.K.S.; formal analysis, A.R.M., K.S.R, N.K, P.K.S., S.Z. and S.K.; investigation, A.R.M., K.S.R, N.K, P.K.S., S.Z. and S.K.S; resources, A.R.M., K.S.R, N.K, and S.K.S; data curation, A.R.M., K.S.R, N.K, and S.K.S; writing—original draft preparation, A.R.M., K.S.R, N.K, P.K.S., S.Z. and S.K.S; writing—review and editing, A.R.M., K.S.R, N.K, P.K.S., S.Z., and S.K.S; visualization, A.R.M., K.S.R, N.K, P.K.S., S.Z. and S.K.S; supervision, K.S.R, N.K, P.K.S., S.Z. and S.K.S.; project administration, K.S.R, and S.K.S.; funding acquisition, K.S.R, and S.K.S. All authors have read and agreed to the published version of the manuscript.

Declaration of Conflict of Interest: The authors declare that they have no known conflicts of financial interests or personal relationships that could have appeared to influence the work reported in this paper. This research is in compliance with the ethical standards and conduct of the journal.